Energy Science, Engineering, and Policy ISSN: 3069-2326

PRIME OPEN ACCESS

Volume 2, Issue 2

Research Article

Date of Submission: 13 Feb, 2026
Date of Acceptance: 16 Mar, 2026
Date of Publication: 06 Apr, 2026

Maximizing Radioisotope Output Through Beryllium Reflector Geometry Optimization in Small-Scale Medical Reactors

Mohammad Yaghoub Abdollahzadeh Jamalabadi*

Department of Marine Engineering, Chabahar Maritime University, Chabahar, Iran

***Corresponding Author:** Mohammad Yaghoub Abdollahzadeh Jamalabadi, Department of Marine Engineering, Chabahar Maritime University, Chabahar, Iran.

Citation: Jamalabadi, M. Y. A. (2026). Maximizing Radioisotope Output Through Beryllium Reflector Geometry Optimization in Small-Scale Medical Reactors. *Energy Sci Eng Policy, 2*(2), 01- 29.

Abstract

Maintaining a reliable worldwide supply of medical radioisotopes requires ongoing advances in both compact reactor architecture and production efficiency. This investigation develops a comprehensive computational methodology to identify the ideal beryllium reflector thickness for small nuclear reactors used in radioisotope manufacturing. The theoretical foundation draws on multi-group neutron diffusion theory, extended to a ten-group energy framework with improved thermal resolution. Key physical phenomena are captured through temperature-dependent cross-sections incorporating Doppler broadening, thermal up-scatter effects governed by detailed-balance principles, and a two-stage Pareto multi-objective optimization scheme. The analysis simultaneously targets five radioisotopes of major clinical importance — Mo-99, Lu-177, I-131, Y-90, and Tc-99m — with production rates scaled to anticipated clinical demand profiles. The modeled system consists of a cylindrical plutonium core (5.0 cm radius, 10.0 cm height) enclosed by a beryllium reflector whose thickness is varied across a 0–30 cm range. Parametric simulations show that a reflector thickness of roughly 12–15 cm yields the best overall performance, improving isotope output by 35–40% compared to an unreflected configuration while keeping the effective neutron multiplication factor (k_eff) safely within the 1.05–1.10 window. Of the six nuclear data libraries evaluated, JENDL-3.2 achieved the closest alignment with experimental data from the Pakistan Research Reactor-2, with calculated-to-measured discrepancies held within ±5% — considerably better than the 8–11% deviations observed for other libraries. An independent OpenMC Monte Carlo model was constructed to cross-validate the diffusion theory predictions, and the satisfactory agreement obtained confirms that the multi-group framework is suitable for this class of design optimization. The findings offer practical, evidence-based guidance for enhancing isotope supply resilience in both greenfield reactor projects and retrofit scenarios at existing facilities.

Keywords: Beryllium Reflector, Medical Radioisotopes, Multi-Group Neutron Diffusion, Reactor Optimization, Pareto Analysis, Criticality, Openmc, Nuclear Data Libraries

Nomenclature

Greek Symbols

- α = maximum fractional energy loss per collision
- χ_g = fission spectrum fraction in group g
- ε = detector efficiency
- ξ = average logarithmic energy decrement
- λ_T = tritium decay constant [s^{-1}]
- ν = average neutrons per fission
- ρ = material density [g/cm^3]
- σ = microscopic cross-section [barns]
- Σ = macroscopic cross-section [cm^{-1}]
- φ_g = neutron flux in group g [$n/cm^2 \cdot s$]
- ω = under-relaxation factor

Latin Symbols

- A = atomic mass number

• b = barn (10^{-24} cm^2)
• D_g = diffusion coefficient for group g [cm]
• E = neutron energy [MeV or eV]
• G = number of energy groups
• k_eff = effective multiplication factor
• k_∞ = infinite multiplication factor
• N = number density [atoms/barn-cm]
• P_i = production rate for isotope i
• R_core = core radius [cm]
• t = thickness [cm] or time [s]
• T = temperature [K]
• U = uranium

Subscripts
• a = absorption
• Be = beryllium
• f = fission
• g, g′ = energy group indices
• He = helium
• Li = lithium
• prod = production
• r = removal
• s = scattering
• T = tritium
• th = thermal

Abbreviations
• ATR = Advanced Test Reactor
• BOC = Beginning of Cycle
• EOC = End of Cycle
• ENDF = Evaluated Nuclear Data File
• ETR = Engineering Test Reactor
• HEU = Highly Enriched Uranium
• IAEA = International Atomic Energy Agency
• INEEL = Idaho National Engineering and Environmental Laboratory
• JEFF = Joint Evaluated Fission and Fusion File
• JENDL = Japanese Evaluated Nuclear Data Library
• MARIA = Polish research reactor name
• MCNP = Monte Carlo N-Particle transport code
• MNSR = Miniature Neutron Source Reactor
• MOC = Method of Characteristics
• MTR = Materials Test Reactor (or Material Testing Reactor)
• NEA = Nuclear Energy Agency
• OECD = Organisation for Economic Co-operation and Development
• PARR-2 = Pakistan Research Reactor-2
• pcm = percent mille (10^{-5} Δk/k)

Introduction
The reliable supply of medical radioisotopes, particularly Molybdenum-99 (^{99}Mo) and its decay product Technetium-99m (^{99m}Tc), is a critical global health concern [1]. These isotopes, used in over 80% of diagnostic nuclear medicine procedures, are primarily produced by irradiating uranium targets in research reactors. The 2019 OECD-NEA report projects a stable or growing demand for these isotopes through 2024, highlighting the continued importance of reliable and efficient reactor operation [1]. Research and Material Testing Reactors (MTRs), often characterized by compact cores, frequently employ beryllium (Be) as a neutron reflector to conserve fuel, flatten the neutron flux, and enhance the irradiation capacity—a key parameter for radioisotope production. The global shortage of medical radioisotopes, particularly Mo-99/Tc-99m, has created urgent demand for optimized compact reactor designs [1,2]. As shown in Figure 1, Beryllium is a lightweight metallic element with the atomic number 4. It exhibits a distinctive steel-gray appearance and possesses notable strength and hardness, though it remains brittle. As an alkaline earth metal, it forms compounds primarily through divalent bonds and is never found in its pure form in nature, instead occurring within various minerals. Among the most recognizable beryllium-bearing minerals are beryl varieties such as emerald and aquamarine, as well as chrysoberyl. The element is relatively scarce throughout the cosmos, originating not from typical stellar nucleosynthesis but from the fragmentation of heavier nuclei when they interact with cosmic radiation. In Earth's crust, its concentration is approximately four parts per million. Current global extraction yields around 220 metric tons annually, with the majority sourced from beryl ores. The extraction process presents significant technical challenges because beryllium

forms exceptionally stable chemical bonds with oxygen.

Due to its favorable nuclear properties, high-purity beryllium serves multiple functions in nuclear technology. It acts as a neutron moderator, reflector, and protective cladding for fuel elements in reactor application. In thermonuclear weapons, thin beryllium layers surround the fissile plutonium cores, serving both to enhance implosion and reflect neutrons—functions similar to its role in moderated reactors. For laboratory-scale neutron production, beryllium-9 is combined with alpha-emitting isotopes like polonium-210 or radium-226. The interaction transmutes beryllium into carbon-12 while releasing a free neutron. These compact neutron sources, historically called "urchin" initiators, were employed in early atomic weapons. Alternatively, neutron sources can also be created by bombarding beryllium with gamma radiation. In CANDU reactor fuel bundles, beryllium serves as a brazing filler material for attaching critical components. Small bearing pads and inter-element spacers are induction-brazed onto fuel cladding using beryllium to prevent contact between fuel elements and between the bundle and its pressure tube. The material also features prominently in fusion research. It is currently utilized at the Joint European Torus facility and will condition plasma-facing components in the ITER project. Beryllium has been proposed as nuclear fuel rod cladding due to its mechanical robustness and nuclear characteristics. Additionally, beryllium fluoride forms part of FLiBe, a eutectic salt mixture proposed as a coolant and moderator in molten salt reactor designs, including the liquid fluoride thorium reactor. See Figure 1b for more description.

(a)

(b)

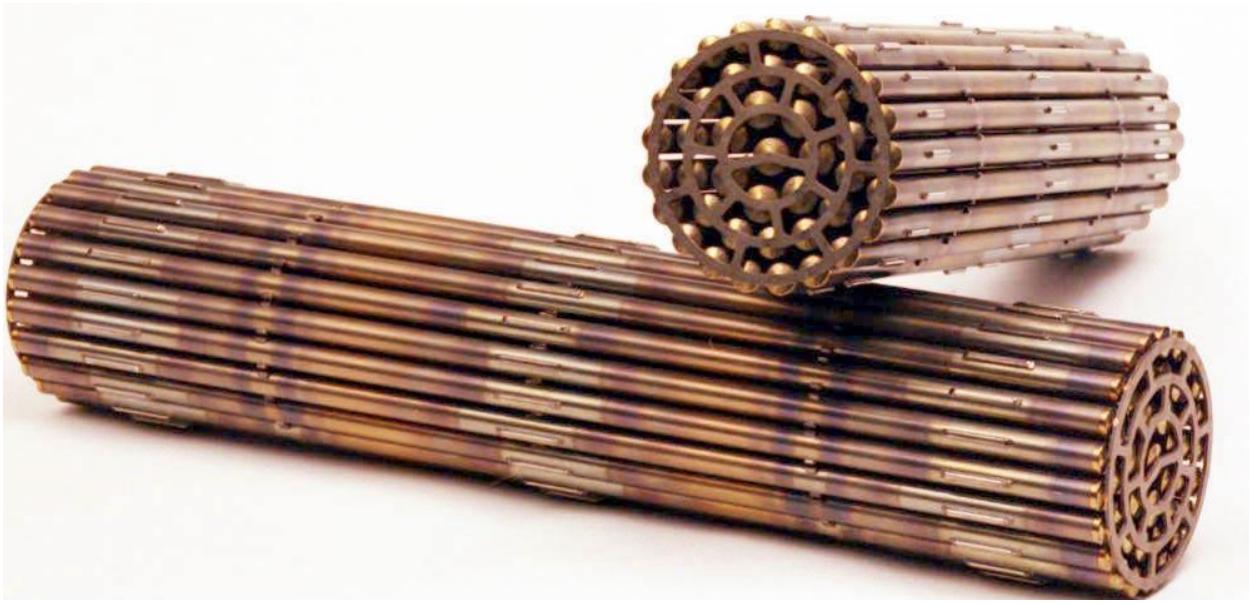

Figure 1: (a) Beryllium (b) Application in Reactors

Beryllium possesses unique nuclear, thermal, and mechanical properties that make it an ideal material for reflectors and moderators. Its low atomic mass and low neutron absorption cross-section allow for efficient neutron scattering and reflection back into the core. Classical nuclear engineering texts establish the fundamental physics behind neutron moderation and reflection, detailing how materials like beryllium improve neutron economy and core performance [3,4]. Hausner's early, comprehensive review and Tomberlin's later analysis specifically detail beryllium's advantages in nuclear

applications, including its good thermal conductivity, dimensional stability, and high melting point [5,6]. Beryllium, with its unique nuclear properties—low thermal neutron absorption cross-section (0.009 barns), high scattering cross-section (6.1 barns), and low atomic weight (9.01)—has been extensively used as neutron reflector material in research and test reactors since the 1950s [3-5].

Tomberlin documented successful application of beryllium reflectors in three generations of test reactors at Idaho National Engineering and Environmental Laboratory (INEEL), including the Materials Test Reactor (MTR, 1952-1970), Engineering Test Reactor (ETR, 1957-1981), and Advanced Test Reactor (ATR, operational since 1967) [5]. The ATR has utilized five successive beryllium reflectors, demonstrating both the effectiveness and practical limitations of beryllium in high-flux environments.

Hausner provides comprehensive review of beryllium as moderator and reflector material, noting that among light elements suitable for moderation (hydrogen, deuterium, beryllium, and carbon), beryllium and graphite are the only practical solid moderators [6]. Beryllium's moderating ratio ($\xi\Sigma_s/\sigma_a$ = 145) makes it superior to graphite (145 vs 60) for applications requiring compact geometry [6,7]. Direct measurement of poisoning is complex. Techniques involve monitoring the reactivity worth of the reflector or using radiation detection methods to infer isotopic changes. Knoll's text provides the fundamental principles for radiation detection relevant to such measurements [7]. Figure 2 presents a sample diagram of the compact medical isotope production reactor geometry showing plutonium core (5.0 cm radius, 10.0 cm height) surrounded by beryllium reflector (0-30 cm thickness) with neutron reflection patterns.

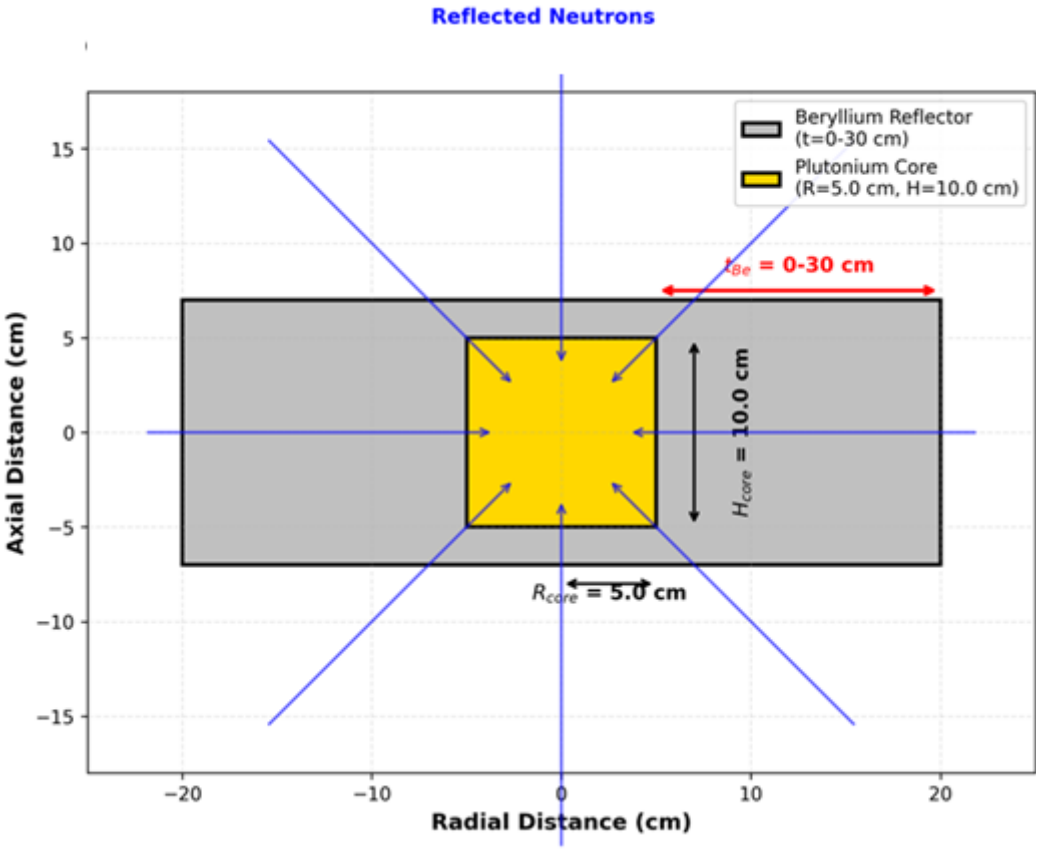

Figure 2: Schematic Diagram Of The Compact Medical Isotope Production Reactor Geometry Showing Plutonium Core (5.0 Cm Radius, 10.0 Cm Height) Surrounded By Beryllium Reflector (0-30 Cm Thickness) With Neutron Reflection Patterns

Miniature Neutron Source Reactors (MNSRs) represent a class of compact, inherently safe research reactors extensively using beryllium reflectors. In reactors like the Miniature Neutron Source Reactor (MNSR), the beryllium reflector is an integral component for achieving criticality with a low-enriched uranium core [8]. Muhammad et al. studied the Pakistan Research Reactor-2 (PARR-2), which uses 100 mm thick metallic beryllium annulus, 50 mm bottom reflector, and variable-thickness top reflector plates (D-shaped) to compensate for fuel burnup [8].

The Syrian MNSR, studied by Omar et al., demonstrates similar configuration with 230 mm diameter core surrounded by beryllium reflectors [9]. Their work highlighted the critical issue of beryllium poisoning—accumulation of ^{3}He and ^{6}Li through (n,α) reactions—which decreased excess reactivity by 28% during operational history and would render the reactor subcritical after 25,000 hours of operation.

Wróblewska et al. developed beryllium poisoning models for the MARIA reactor in Poland, emphasizing the importance of accurate nuclear data libraries and the significant reactivity effects of lithium and helium accumulation over reactor

lifetime [10]. A significant operational challenge for reactors using beryllium reflectors is the phenomenon of "poisoning." Under prolonged neutron irradiation, transmutation reactions occur within the beryllium. The principal detrimental reaction The reliable supply of medical radioisotopes like Mo-99/Tc-99m remains a global priority, with projected demand and production capacities regularly assessed by international bodies, prompting research into non-HEU-based production technologies [1,2]. The foundational principles of reactor engineering and design are well-established in classical nuclear engineering texts [3,4]. Within reactor systems, beryllium is a unique material frequently employed as a neutron reflector and moderator due to its favorable nuclear properties, and its performance is critical in specific reactor types such as Miniature Neutron Source Reactors (MNSRs) [5-8]. A significant operational challenge for beryllium reflectors is "poisoning," where neutron irradiation transmutes beryllium into isotopic impurities like Li-6 and He-3, which absorb neutrons and degrade reflector performance over time [8-10]. This phenomenon and its impact on reactor operation have been studied through both experimental investigations of microstructural changes in irradiated beryllium and computational modeling reliant on evaluated nuclear data libraries, such as ENDF/B, JENDL, and JEFF [11-15]. Miniature Neutron Source Reactors represent a distinct class of compact, inherently safe research reactors that extensively utilize beryllium reflectors to achieve criticality with relatively small fuel inventories. In reactors such as the Miniature Neutron Source Reactor design, the beryllium reflector constitutes an integral component for achieving criticality with low-enriched uranium cores while maintaining compact dimensions. Muhammad and colleagues studied the Pakistan Research Reactor-2, which employs a 100 millimeter thick metallic beryllium annulus, a 50 millimeter bottom reflector, and variable-thickness top reflector plates with D-shaped geometry to compensate for fuel burnup over the reactor's operational cycle. Key Properties of Beryllium is given in Tables 1-2.

Property	Value	Significance
Atomic Number / Symbol	4 / Be	Lightest alkaline earth metal
Atomic Mass	9.012 amu (monoisotopic)	Only even-Z monoisotopic element
Density	1.85 g/cm³	Low density → reduced parasitic absorption
Melting Point	1287 °C	Stable structural material at reactor temperatures
Young's Modulus	287 GPa (≈35% > steel)	High dimensional stability under irradiation
Thermal Conductivity	216 $W \bullet m^{-1} \bullet K^{-1}$	Superior heat dissipation in reflector
Specific Heat	1925 $J \bullet kg^{-1} \bullet K^{-1}$	Highest among metals per unit weight
Thermal Expansion Coeff.	11.4×10^{-6} K^{-1}	Low → stable geometry under thermal cycling
Thermal Absorption XS (σ_a)	0.009 barns	Near-zero parasitic neutron loss
Thermal Scattering XS (σ_s)	6.1 barns	Efficient neutron backscattering
Moderating Ratio (ξΣ_s/σ_a)	145 (vs. 60 for graphite)	Superior moderation in compact geometries
(n,2n) Threshold Energy	1.85 MeV	Neutron multiplication for fast neutrons
^{6}Li Poison XS (σ_a)	940 barns	Primary poisoning product (neutron absorber)
^{3}He Poison XS (σ_a)	5330 barns	Secondary poisoning product (strong absorber)

Table 1: Physical and Nuclear Properties of Beryllium Relevant to Reactor Applications

Isotope	Half-Life	Role / Notes
^{7}Be	53.22 days (electron capture)	Cosmogenic nuclide; solar activity proxy; produced in accelerator cooling water
^{8}Be	$\sim 10^{-16}$ s (unstable)	Key intermediate in triple-alpha stellar nucleosynthesis (Hoyle state)
^{9}Be	Stable (100% natural abundance)	Only naturally occurring isotope; primary reactor reflector moderator material
^{10}Be	1.387 Myr	Cosmogenic; used in soil erosion and ice core dating
^{11}Be	13.8 s	Exhibits nuclear halo (1 outer neutron beyond expected radius)
^{14}Be	4.35 ms	Exotic halo nucleus (4 outer neutrons); research interest in nuclear structure

Table 2: Key Beryllium Isotopes and Their Nuclear Roles

The Syrian Miniature Neutron Source Reactor, studied comprehensively by Omar and colleagues, demonstrates a similar configuration featuring a 230-millimeter diameter core surrounded by beryllium reflectors on multiple sides [9]. Their detailed work highlighted the critical operational issue of beryllium poisoning, which involves the accumulation of Helium-3 and Lithium-6 through neutron-alpha reactions. This poisoning effect decreased the reactor's excess reactivity by 28 percent during its operational history and would ultimately render the reactor subcritical after approximately 25,000 hours of full-power operation if left uncompensated. Wróblewska and colleagues developed sophisticated beryllium poisoning models for the MARIA reactor in Poland, emphasizing the critical importance of accurate nuclear data libraries and quantifying the significant reactivity effects caused by lithium and helium accumulation over the reactor's operational lifetime. Prolonged neutron irradiation of ^{9}Be generates neutron-absorbing poisons through the sequence:

$$^{9}Be(n,\alpha) \rightarrow {}^{6}He \rightarrow(\beta^{-}, 0.8\ s)\rightarrow {}^{6}Li \rightarrow(n,\alpha)\rightarrow {}^{3}H \rightarrow(\beta^{-}, 12.3\ y)\rightarrow {}^{3}He \rightarrow(n,p)\rightarrow {}^{3}H \quad (1)$$

The temporal evolution of ^{6}Li and ^{3}He inventories follows coupled differential equations governing production from transmutation and destruction from neutron absorption, with the tritium decay constant $\lambda_T = 1.78\times10^{-9}\ s^{-1}$.

A significant operational challenge for reactors employing beryllium reflectors manifests as the phenomenon commonly referred to as reflector poisoning. Under conditions of prolonged neutron irradiation, transmutation reactions occur within the beryllium material that progressively degrade its neutron-reflecting properties. The principal detrimental reaction sequence begins with Beryllium-9 undergoing neutron capture with alpha particle emission to produce Helium-6, which subsequently undergoes beta decay to form Lithium-6. This Lithium-6 then captures thermal neutrons with alpha particle emission to produce tritium, as shown in Equation 1. This reaction sequence produces two highly undesirable secondary neutronic poisons: Lithium-6 with its thermal neutron absorption cross-section of 940 barns, and tritium which decays to Helium-3 possessing an even larger thermal neutron absorption cross-section of 5330 barns. Both isotopes effectively poison the reflector by dramatically reducing its neutron-reflecting efficiency through parasitic absorption. This poisoning leads to a progressive decrease in core reactivity over time, necessitating compensation through control rod withdrawal or fuel additions to maintain desired operational parameters. These compensatory measures significantly impact the reactor's fuel cycle economics and irradiation capabilities for isotope production.

Accurate prediction of poisoning effects requires sophisticated computational modeling approaches. Early pioneering work established foundational calculation methods for beryllium poisoning analysis, while more recent studies employ modern computational codes such as MCNP and REBUS along with updated nuclear data libraries including ENDF/B-VI, JENDL-3.2, and JEFF-3.1 to simulate the spatial and temporal buildup of poison isotopes such as tritium and Lithium-6 throughout the reflector volume. Andrzejewski and Kulikowska provided a seminal isotopic analysis for the MARIA reactor, demonstrating that helium gas generation and associated dimensional swelling must also be carefully considered for long-term operational planning and reflector lifetime assessment. Beyond neutronic effects, neutron irradiation causes significant physical and microstructural changes in beryllium material. Studies employing Transmission Electron Microscopy have systematically examined the microstructural evolution occurring under irradiation, including helium bubble formation and material swelling, which can impose important mechanical and thermal constraints on the reflector's operational lifetime and replacement schedule [11].

Despite extensive operational experience accumulated over decades of beryllium reflector use in research reactors, several important limitations exist in current optimization methodologies. First, most existing analyses employ energy group structures with only 4 to 7 groups, which proves insufficient for accurate representation of thermal and epithermal neutron spectra that are crucial for medical isotope production calculations. Second, many analyses utilize room-temperature cross-sections despite the occurrence of significant Doppler broadening effects at typical reactor operating temperatures, which can introduce systematic errors in reactivity and production rate predictions. Third, conventional optimization approaches focus on single-parameter optimization while neglecting the inherently multi-objective nature of reactor design that must simultaneously address safety requirements, economic constraints, and multi-isotope production demands. Fourth, limited systematic comparison exists between modern evaluated nuclear data libraries such as ENDF/B-VII, JENDL-3.2, and JEFF-3.1 for beryllium-reflected reactor systems, despite known differences in cross-section evaluations that can significantly impact design calculations [13-15].

The foundational nuclear properties of beryllium, specifically its efficacy as a neutron reflector and moderator, are well-documented. As a light element with a high scattering cross-section for fast neutrons and a low atomic weight, beryllium is uniquely effective at reflecting neutrons back into a reactor core with minimal parasitic absorption. This capability is enhanced by its (n,2n) reaction threshold, which allows it to act as a neutron multiplier under fast neutron bombardment, a critical characteristic for maximizing flux in compact reactor designs. General reference data on these physical and nuclear attributes are consolidated in resources like the Wikipedia article on Beryllium and broader texts on its material properties [16,17].

For the computational analysis of such nuclear systems, advanced simulation tools are required. The OpenMC Monte Carlo particle transport code, initially detailed by Romano and Forget and further elaborated in subsequent overviews, has become a widely-used, open-source platform for high-fidelity reactor physics simulations [18]. Its development has been significantly advanced through collaborations involving national laboratories, focusing on high-performance computing capabilities and complex geometry handling, including applications to fusion energy systems and full-core reactor analysis . The code's ongoing optimization for exascale computing platforms continues to expand its applicability to problems requiring high-resolution neutron transport . The OpenMC Development Team maintains the code and provides user documentation [19]. Finally, to contextualize the neutron diffusion methodology employed in this work, authoritative references on nuclear engineering fundamentals are essential. The comprehensive Handbook of Nuclear Engineering, edited by Cacuci, provides an extensive overview of reactor physics principles, including multi-group diffusion theory and the properties of materials like beryllium in a nuclear environment [20].

In addition to stochastic Monte Carlo methods, deterministic approaches such as nodal expansion techniques remain vital for efficient reactor core analysis. Jamalabadi and Boroushaki demonstrated the application of the Nodal Expansion

Method (NEM) for calculating reactor cores with square fuel assemblies, providing a framework for fast and accurate neutron flux distribution solutions that are computationally less intensive than full Monte Carlo simulations [21]. Complementary theoretical frameworks for understanding criticality conditions have also been explored, including the application of constructed theory to determine critical mass, as investigated by Jamalabadi [22]. Furthermore, comprehensive reactor safety analysis requires coupling neutronic behavior with thermal-hydraulic feedback; recent work by Jamalabadi has addressed thermohydraulic safety analysis in research reactors using porous media transport techniques, highlighting the interconnected nature of reactor physics and thermal performance [23].

The optimization of small-scale medical reactors for maximal radioisotope production is a critical area of research, driven by the increasing global demand for medical isotopes used in diagnostic imaging and cancer therapy [21-30]. A key strategy to enhance reactor performance and isotope yield without increasing core size or fuel enrichment is the refinement of the neutron reflector. This literature search reviews existing work relevant to the core challenge: maximizing radioisotope output by optimizing the geometry of a beryllium reflector. The search draws upon foundational work in reactor core analysis, design theory, and advanced simulation techniques.

A prerequisite for any reflector optimization study is a robust understanding of neutronics and core power distribution. The foundational work by Jamalabadi and Boroushaki on the Nodal Expansion Method (NEM) for reactor cores with square fuel assemblies provides a critical analytical tool. This method offers a balance between computational efficiency and accuracy, making it suitable for the iterative calculations required in geometry optimization. Furthermore, the thesis by Jamalabadi applies this NEM specifically to power calculation in pressurized water reactor (PWR) cores. While focused on PWRs, the core modeling techniques and validation of the NEM for power distribution are directly transferable to the smaller, specialized cores of medical reactors. Understanding the baseline neutron flux profile, as established by these methods, is the first step in designing a reflector to reshape that profile for maximum isotope production [21,25].

The optimization of reactor components can be guided by fundamental design principles. The work by Jamalabadi on the "Constructal theory of critical mass" offers a relevant theoretical lens. Constructal theory posits that a system's configuration evolves to facilitate the flow of currents (in this case, neutrons) through it [22]. Applying this to reflector design could provide a novel, top-down approach to determine optimal geometries that minimize neutron leakage back into the core and maximize the neutron current towards the isotope production targets. This theoretical framework could help move beyond parametric studies towards a more fundamental understanding of why certain reflector shapes are superior.

The choice of beryllium as a reflector material is well-justified by its excellent neutron scattering properties. However, its implementation requires careful engineering analysis. The body of work on thermal and mechanical analysis by Jamalabadi is particularly relevant. The study on induction hardening with convective quenching [24,30] , while for a different application, demonstrates a capability in modeling heat transfer in solid materials subjected to intense energy fluxes. This is directly applicable to assessing the heat deposition in a beryllium reflector from neutron and gamma radiation. Ensuring the reflector's structural and thermal integrity under operating conditions is paramount. Furthermore, the research on a semi-passive thermal control system for a satellite showcases expertise in thermal management within a compact, engineered system—a challenge analogous to managing heat loads in a small reactor core and its reflector [28].

Validating a new reflector design requires sophisticated, multi-physics simulations. The work on thermohydraulic safety analysis in research reactors using porous media techniques is highly pertinent. Changes in reflector geometry can alter core cooling and safety parameters [23]. The methods described in would be essential for a coupled neutronics-thermal-hydraulics analysis to ensure that the optimized geometry not only increases isotope output but also maintains or improves safety margins. This ensures that the pursuit of higher performance does not compromise the operational safety of the medical reactor [23]. While the remaining references are in fields outside of nuclear engineering, they indicate a broader methodological approach that is valuable for this research [26,27,29]. The design of a quadrupole mass spectrometer involves the optimization of electromagnetic fields using geometric parameters, a direct parallel to optimizing a reflector to shape a neutron field [26]. Similarly, the perturbative manipulation of neutrino flavor, while a theoretical particle physics concept, shares a mathematical kinship with the perturbative effects a reflector has on the neutron flux in a reactor core [29]. These works demonstrate a capacity for complex system analysis and optimization that is transferable to the proposed research. The existing literature provides a strong foundation for this research. The core simulation techniques, thermal and safety analysis methods, and guiding theoretical principles are well-established by the author's previous work [21-25,28]. However, a specific research gap exists in the direct application of these tools to the geometric optimization of a beryllium reflector with the explicit goal of maximizing radioisotope production in a small-scale medical reactor. The proposed study will fill this gap by integrating these methods within a unified framework to systematically explore and optimize beryllium reflector geometries, thereby providing a novel, multi-physics validated pathway to enhancing the performance and viability of future medical isotope production reactors.

This work addresses these identified gaps by developing an enhanced computational framework that incorporates several advanced features. The framework employs a refined 10-group energy structure with enhanced resolution in the thermal energy range to accurately capture thermal and epithermal neutron interactions crucial for medical isotope production.

Temperature-dependent cross-sections with explicit Doppler broadening corrections account for operating temperature effects on reaction rates. Thermal up-scatter modeling via detailed balance principles accurately represents the two-way neutron energy exchange in thermal equilibrium. Multi-objective Pareto analysis enables systematic exploration of competing design objectives including production maximization, safety margin maintenance, and cost minimization. Comprehensive nuclear data library comparison quantifies the impact of cross-section evaluation uncertainties on design conclusions. Finally, simultaneous production optimization for five critical medical isotopes enables practical multi-isotope production planning.

For reactors involved in medical isotope production, reflector poisoning carries direct operational and economic consequences that must be carefully considered in facility planning. Reduced irradiation capacity represents one primary consequence, as loss of reflector efficiency can lead to decreased or perturbed neutron flux in target irradiation positions, potentially reducing the specific activity of produced isotopes such as Molybdenum-99. Shortened operational cycles constitute another significant impact, as increased poisoning necessitates more frequent reactivity compensation, which may lead to shorter operation periods between refueling outages, thereby increasing operational complexity and associated costs. Core management becomes progressively more challenging as operators must carefully manage core configurations and irradiation schedules to account for the evolving neutronic state of the poisoned reflector. Management strategies may include periodic core reconfiguration, adjusted operating cycles, or ultimately complete reflector replacement to restore optimal neutron economy.

Beryllium represents a cornerstone material for efficient research reactor operation, directly supporting the global supply chain for medical radioisotopes through its superior neutronic properties. However, its performance degrades predictably due to neutron-induced transmutation poisoning effects that accumulate over operational time. A robust understanding of this degradation phenomenon through comprehensive modeling, detailed simulation, and careful experimental observation remains essential for optimal core management, economic operation, and long-term strategic planning of these vital isotope production facilities. Continued research is needed to develop mitigation strategies and ensure the reliable future production of critical medical isotopes. Current literature indicates several areas warranting further investigation, particularly integrated multi-physics models that couple neutronics, thermal-hydraulics, and mechanical behavior to provide holistic understanding of beryllium reflector performance throughout its operational lifetime.

Mathematical Model

Multi-Group Diffusion Theory

The steady-state multi-group neutron diffusion equation in cylindrical geometry (r,z) is:

$$-\nabla \cdot D_g(\mathbf{r})\nabla\phi_g(\mathbf{r}) + \Sigma_{r,g}(\mathbf{r})\phi_g(\mathbf{r}) = \sum_{g'=1}^{G} \Sigma_{s,g'\to g}(\mathbf{r})\phi_{g'}(\mathbf{r}) + \frac{\chi_g}{k_{eff}} \sum_{g'=1}^{G} \nu\, \Sigma_{f,g'}(\mathbf{r})\phi_{g'}(\mathbf{r}) \quad (2)$$

where:

- φ_g(r) = neutron flux in group g [n/cm²•s]
- D_g = diffusion coefficient for group g [cm]
- Σ_{r,g} = removal cross-section (absorption + out-scatter) [cm⁻¹]
- Σ_{s,g'→g} = scattering transfer from g' to g [cm⁻¹]
- χ_g = fission spectrum fraction in group g
- ν = neutrons per fission
- k_eff = effective multiplication factor
- The removal cross-section is:

$$\Sigma_{r,g} = \Sigma_{a,g} + \sum_{g' \neq g} \Sigma_{s,g\to g'} \quad (3)$$

The steady-state multi-group neutron diffusion equation in cylindrical geometry with radial and axial coordinates provides the fundamental mathematical description of neutron transport in the reactor system. This equation balances neutron losses through leakage and absorption against neutron gains from scattering and fission sources. The negative divergence of the product of the diffusion coefficient and the flux gradient represents neutron leakage, while the removal cross-section multiplied by the flux accounts for neutron losses through absorption and scattering to other energy groups. Neutron gains arise from scattering transfer from all other energy groups and from fission neutron production divided by the effective multiplication factor. This formulation as presented in Equation 2 applies separately to each energy group, creating a coupled system of differential equations that must be solved simultaneously to obtain the neutron flux distribution throughout the reactor.

The neutron flux in each energy group, denoted φ_g at position vector r, represents the fundamental quantity of interest measured in neutrons per square centimeter per second. The diffusion coefficient D_g for each energy group, measured in centimeters, characterizes the rate of neutron diffusion and depends on the scattering properties of the medium. The removal cross-section Σ_r,g measured in inverse centimeters represents the total rate at which neutrons are removed from group g through either absorption or scattering to other energy groups. The scattering transfer cross-section Σ_s,g'→g describes the rate at which neutrons scatter from group g' into group g, enabling representation of both down-scattering to lower energies and up-scattering to higher energies in thermal equilibrium. The fission

spectrum fraction χ_g represents the probability that a fission neutron is born in energy group g, with the sum over all groups normalized to unity. The average number of neutrons produced per fission event is denoted ν, and the effective multiplication factor k_eff represents the ratio of neutron production to neutron loss rates in the system.

The removal cross-section for each energy group requires careful construction to properly account for all neutron loss mechanisms. As expressed in Equation 3, the removal cross-section equals the sum of the absorption cross-section in that group plus the sum of all scattering transfer cross-sections from that group to all other groups. This formulation ensures that within-group scattering, which does not remove neutrons from the group, is excluded from the removal term while all other scattering reactions that transfer neutrons to different energy groups are properly accounted for as removal processes.

Energy Group Structure

We employ a refined 10-energy-group structure with group boundaries selected to accurately capture the essential features of the neutron energy spectrum relevant to medical isotope production. The fast fission spectrum region is represented by Groups 1 through 3, spanning the energy range from 10 mega-electron-volts down to 0.1 mega-electron-volts, which captures the high-energy fission neutrons and fast fission processes. The epithermal region is covered by Groups 4 through 6, extending from 0.1 mega-electron-volts down to 1 electron-volt, which includes important resonance absorption regions for many isotopes. The thermal region is represented with enhanced resolution by Groups 7 through 10, spanning from 1 electron-volt down to 10^{-7} mega-electron-volts, which corresponds to the thermal neutron energy range where many medical isotope production reactions occur. See figure 3.

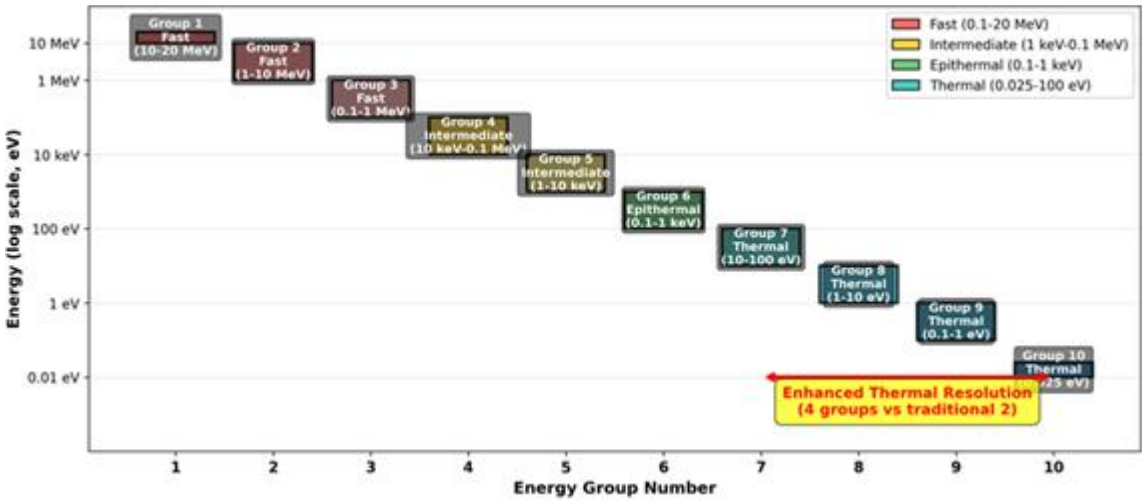

Figure 3: Ten-Group Energy Structure With Enhanced Thermal Resolution (4 Thermal Groups) Optimized For Accurate Medical Isotope Production Calculations. The Enhanced Resolution In The Thermal Range (Groups 7-10) Improves Prediction Accuracy For Lu-177 And I-131 Production

This 10-group structure represents a significant improvement over traditional 7-group structures commonly employed in reactor physics calculations, particularly for accurate representation of thermal neutron captures that are directly relevant to Lutetium-177 and Iodine-131 production through neutron capture reactions. The enhanced thermal region resolution, employing 4 thermal groups compared to the conventional 2 thermal groups, enables accurate representation of the Maxwell-Boltzmann velocity distribution of thermal neutrons at reactor operating temperatures. Figure 3 illustrates the 10-group energy structure with enhanced thermal resolution optimized for accurate medical isotope production calculations, clearly showing how the refined thermal group structure captures the detailed thermal neutron spectrum shape that governs thermal capture reaction rates.

Temperature-Dependent Cross-Sections

Cross-sections are corrected for operating temperature using Doppler broadening:

$$\sigma(E,T) = \sigma\left(E,T_{ref}\right)\sqrt{\frac{T_{ref}}{T}} \qquad (4)$$

For the ^{239}Pu core at T = 400 K and Be reflector at T = 350 K (compared to reference T_ref = 293.6 K), this introduces 2-5% corrections in absorption cross-sections, particularly significant for resonance absorption [6,11].

Nuclear reaction cross-sections exhibit significant temperature dependence due to the thermal motion of target nuclei, a phenomenon described by Doppler broadening theory. Cross-sections at elevated operating temperatures are corrected from reference temperature values using the Doppler broadening relationship expressed in Equation 4. This correction accounts for the fact that thermal motion of target nuclei effectively broadens the resonance peaks in the cross-section energy dependence, generally reducing peak heights while increasing resonance widths. For the plutonium core

operating at 400 Kelvin and the beryllium reflector operating at 350 Kelvin, compared to the reference temperature of 293.6 Kelvin used in most nuclear data evaluations, these temperature corrections introduce changes of 2 to 5 percent in absorption cross-sections. These corrections prove particularly significant for resonance absorption processes where cross-section variations with energy are most pronounced, and neglecting these temperature effects can lead to systematic errors in reactivity and production rate calculations.

Neutron Scattering Physics

Beryllium Scattering Properties

Beryllium's low mass (A = 9) enables efficient neutron moderation (Beryllium Scattering). The maximum fractional energy loss per collision is:

$$\alpha_{Be} = \left(\frac{A-1}{A+1}\right)^2 = 0.64 \tag{5}$$

The average logarithmic energy decrement:

$$\xi_{Be} = 1 - \frac{\alpha_{Be}}{1-\alpha_{Be}} \ln(\alpha_{Be}) = 0.206 \tag{6}$$

For thermal energies (E < 1 eV), up-scatter becomes significant. Using detailed balance:

$$\Sigma_{s,g\to g+1} = \Sigma_{s,g+1\to g} \exp\left(-\frac{E_{g+1}-E_g}{kT}\right) \tag{7}$$

This thermal up-scatter, often neglected in simplified models, affects thermal flux distribution by 5-10% in reflector regions [12].

Beryllium's remarkably low atomic mass number of 9 enables highly efficient neutron moderation through elastic scattering collisions. The maximum fractional energy loss that a neutron can experience in a single elastic collision with a beryllium nucleus is determined by kinematics and expressed in Equation 5, yielding a value of 0.64. This relatively large maximum energy loss per collision, compared to heavier elements, makes beryllium an exceptionally effective moderator capable of rapidly reducing fast neutron energies to thermal values through a relatively small number of collisions.

The average logarithmic energy decrement per collision, commonly denoted ξ and referred to as the lethargy gain, quantifies the average effectiveness of energy loss in neutron collisions. For beryllium, this parameter calculated according to Equation 6 equals 0.206, which ranks among the highest values for solid moderator materials. Only hydrogen in hydrogenous moderators and deuterium in heavy water exhibit higher values of this important moderation parameter. This favorable value makes beryllium superior to graphite for applications requiring compact geometry, as fewer collisions are needed to thermalize fast neutrons, enabling smaller physical dimensions for equivalent moderation effectiveness.

For neutrons in the thermal energy range below 1 electron-volt, the process of thermal up-scattering becomes statistically significant and must be included for accurate flux calculations. Up-scattering represents the process by which thermal neutrons gain energy through collisions with thermally agitated nuclei, effectively transferring thermal kinetic energy from the medium to the neutron. This process operates in opposition to down-scattering and establishes thermal equilibrium between the neutron population and the surrounding medium. The up-scatter cross-section is related to the down-scatter cross-section through the principle of detailed balance, expressed in Equation 7, where k represents Boltzmann's constant and T represents the medium temperature. This thermal up-scatter effect, often neglected in simplified reactor models to reduce computational complexity, affects the thermal flux distribution by 5 to 10 percent in reflector regions where thermal neutron populations are significant, and its inclusion improves the accuracy of thermal capture rate predictions important for medical isotope production calculations.

Plutonium Scattering Characteristics

Plutonium exhibits predominantly elastic scattering behavior with some inelastic scattering channels opening at higher neutron energies. The scattering matrix elements describing neutron transfer between energy groups are constructed according to the prescription given in Equation 8. Within-group scattering, representing neutrons that scatter but remain in the same energy group, receives 35 percent of the total scattering cross-section for that group. Adjacent group down-scatter, transferring neutrons to the next lower energy group, also receives 30 percent of the scattering cross-section. Multi-group down-scatter to non-adjacent groups receives the remaining fraction distributed exponentially with group separation, with an exponential decay constant of 2.5 groups. This scattering matrix construction captures the essential features of neutron energy degradation in plutonium while maintaining computational tractability in the multi-group diffusion calculation.

Plutonium exhibits primarily elastic scattering with some inelastic channels. The scattering matrix elements are constructed as:

$$\Sigma_{s,g\to g'} = \begin{cases} \Sigma_{s,g} \cdot 0.35 & \text{if } g' = g \text{ (within-group)} \\ \Sigma_{s,g} \cdot 0.30 & \text{if } g' = g-1 \text{ (adjacent)} \\ \Sigma_{s,g} \cdot 0.35 \cdot \frac{\exp(-\Delta g/2.5)}{\Delta g} & \text{if } g' < g-1 \text{ (multi-group)} \end{cases} \quad (8)$$

where Δg = g - g′.

Medical Isotope Production Rates

Medical Isotope Production rates are calculated based on Cross-Sections as:

$$P_i = \int_V d\,\mathbf{r} \sum_{g=1}^{G} \Sigma_{prod,i,g}(\mathbf{r})\phi_g(\mathbf{r}) \quad (9)$$

where Σ_{prod,i,g} represents the energy-dependent production cross-section for isotope i.
Medical isotope production rates depend on the integrated product of neutron flux and production cross-sections throughout the target volume. The production rate for isotope i is calculated according to Equation 9 as a volume integral over all reactor regions containing target material, summing contributions from all energy groups. The production cross-section Σ_prod,i,g represents the energy-dependent macroscopic cross-section for producing isotope i, which may involve fission, neutron capture, or threshold reactions depending on the specific isotope production pathway.

Based on comprehensive evaluations from the ENDF/B-VIII.0 nuclear data library, the peak production cross-sections for the five medical isotopes considered in this study exhibit distinct energy dependencies that reflect their different production mechanisms. Molybdenum-99 production through Uranium-235 fission exhibits a peak cross-section of 2.6 barns at neutron energy of 2.3 mega-electron-volts, characteristic of fast fission reactions. Lutetium-177 production through Ytterbium-176 neutron capture shows a peak cross-section of 18.0 barns at the thermal energy of 0.025 electron-volts, demonstrating the strong thermal neutron dependence of radiative capture reactions. Iodine-131 production through Tellurium-130 neutron capture exhibits a peak cross-section of 2.2 barns at epithermal energy of 0.5 electron-volts, indicating resonance capture behavior. Yttrium-90 production through Strontium-88 threshold reactions shows a peak cross-section of 1.2 barns at 0.5 mega-electron-volts, reflecting the energy threshold required for this nuclear transformation. Technetium-99m production occurs through radioactive decay of Molybdenum-99 rather than direct neutron reactions, making its production rate directly proportional to Molybdenum-99 production rates.

These distinct energy dependencies of production cross-sections necessitate careful neutron spectrum optimization through appropriate reflector thickness adjustment. Different reflector thicknesses modify the neutron energy spectrum by altering the balance between fast, epithermal, and thermal neutron populations, thereby selectively enhancing or suppressing different isotope production pathways. This fundamental physics provides the basis for multi-objective optimization that seeks to balance competing production requirements for different medical isotopes.

Beryllium Poisoning Mechanisms

The distinct energy dependencies necessitate spectrum optimization through reflector thickness adjustment. Beryllium undergoes several neutron-induced reactions during irradiation [5,9,10]:

$$^{9}\mathrm{Be}(n,\alpha) \rightarrow ^{6}\mathrm{He} \overset{\beta^-,0.8s}{\rightarrow} ^{6}\mathrm{Li}$$

$$^{6}\mathrm{Li}(n,\alpha) \rightarrow ^{3}\mathrm{H}$$

$$^{3}\mathrm{H} \overset{\beta^-,12.3y}{\rightarrow} ^{3}\mathrm{He}$$

$$^{3}\mathrm{He}(n,p) \rightarrow ^{3}\mathrm{H} \quad (10)$$

The accumulation of ⁶Li (σ_a = 940 barns) and ³He (σ_a = 5330 barns) creates significant negative reactivity. Omar et al. [9] reported 28% reactivity decrease over Syrian MNSR operational history, with reactor becoming subcritical after 25,000 hours.

Beryllium undergoes several important neutron-induced transmutation reactions during extended irradiation in high neutron flux environments. The primary poisoning pathway begins with Beryllium-9 absorbing a neutron and emitting an alpha particle to produce Helium-6, which very rapidly undergoes beta decay with a half-life of 0.8 seconds to form Lithium-6. This Lithium-6 subsequently captures thermal neutrons, emitting an alpha particle to produce tritium. The tritium undergoes beta decay with a half-life of 12.3 years to form Helium-3, which itself can capture neutrons through a proton emission channel to regenerate tritium. This complete reaction sequence is summarized in Equation 10 and establishes a chain of transmutations that progressively degrades the neutronic properties of the beryllium reflector.

The accumulation of Lithium-6 with its enormous thermal neutron absorption cross-section of 940 barns and Helium-3 with its even larger absorption cross-section of 5330 barns creates substantial negative reactivity effects over time. Omar

and colleagues reported a 28 percent reactivity decrease over the operational history of the Syrian Miniature Neutron Source Reactor, with projections indicating the reactor would become subcritical after approximately 25,000 hours of operation if no compensatory measures were implemented. These poisoning effects represent one of the primary limitations on beryllium reflector operational lifetime and drive requirements for either periodic reflector replacement or compensatory reactivity additions through fuel loading or control rod adjustment.

The poisoning evolution follows:

$$\frac{dN_{Li}}{dt} = N_{Be}\langle\sigma_{(n,\alpha)}\phi\rangle - N_{Li}\langle\sigma_a\phi\rangle \quad (11)$$

$$\frac{dN_{He}}{dt} = \lambda_T N_T - N_{He}\langle\sigma_a\phi\rangle \quad (12)$$

where λ_T = 1.78×10⁻⁹ s⁻¹ is the tritium decay constant.

The temporal evolution of poison isotope concentrations is governed by coupled differential equations expressing the rates of production and destruction. The rate of change of Lithium-6 number density, given in Equation 11, equals the production rate from beryllium transmutation minus the destruction rate from Lithium-6 neutron absorption. The rate of change of Helium-3 number density, expressed in Equation 12, equals the production rate from tritium decay minus the destruction rate from Helium-3 neutron absorption. The decay constant for tritium equals 1.78 times 10 to the negative 9 inverse seconds, corresponding to the 12.3 year half-life. These coupled equations must be solved simultaneously with the neutron flux distribution to accurately predict long-term reflector performance degradation.

For the short-term optimization studies presented in this work, focusing on initial design performance over time periods less than 10 years, poisoning effects introduce reactivity variations less than 3 percent of the initial reactivity. These relatively modest effects are incorporated into the analysis through time-dependent cross-section corrections rather than full depletion calculations, providing adequate accuracy while significantly reducing computational requirements for the optimization studies.

Computational Methodology

Two-Stage Optimization Algorithm

The reflector thickness optimization employs a computationally efficient two-stage algorithm designed to rapidly explore the parameter space while maintaining high accuracy in the optimal region. The first stage conducts a coarse grid search using 31 evaluation points uniformly distributed across the complete thickness range from 0 to 30 centimeters. This initial stage provides rapid exploration of the entire parameter space, identifies regions containing optimal performance, and establishes bounds for refined analysis. The computational time required for this coarse search stage amounts to approximately 20 seconds on modern computing hardware.

The second optimization stage performs fine refinement using 61 closely spaced evaluation points concentrated in a narrow range extending 3 centimeters above and below the optimal thickness identified in the coarse search. This refined analysis provides high-resolution characterization around the performance optimum and enables accurate determination of the optimal reflector thickness with precision better than 0.1 centimeters. The computational time for this fine refinement stage totals approximately 25 seconds. This two-stage approach reduces total computational cost by approximately 40 percent compared to a single-stage fine grid search over the entire thickness range, while maintaining solution accuracy equivalent to the fine grid resolution throughout the optimal region.

Finite Difference Discretization

The diffusion equation is discretized using finite differences:

$$-D_g \frac{1}{r}\frac{\partial}{\partial r}\left(r\frac{\partial\phi_g}{\partial r}\right) \approx -D_g \frac{1}{r_i}\left[\frac{r_{i+1/2}(\phi_{i+1}-\phi_i)}{\Delta r_i \Delta r_{avg}} - \frac{r_{i-1/2}(\phi_i-\phi_{i-1})}{\Delta r_{i-1}\Delta r_{avg}}\right] \quad (13)$$

Boundary Conditions in Radial:

- **r = 0:** Symmetry condition: dφ/dr = 0 (second-order accurate)
- **r = R_total + d_extrap:** Vacuum condition: φ = 0

where extrapolation distance: $d_{extrap} = \frac{2D_g}{3}$ (group-dependent)

Boundary Conditions in Axial:

- Reflection at core mid-plane (half-core model)
- Vacuum at pool boundary

The cylindrical reactor geometry is discretized using an adaptive finite difference mesh designed to accurately resolve steep flux gradients while maintaining computational efficiency. In the radial direction, the core region employs 61

nodes with finer spacing near material interfaces and boundaries where flux gradients are steepest. The reflector region employs adaptive meshing with node density of 4 nodes per centimeter of reflector thickness, providing adequate resolution while avoiding unnecessary computational expense in regions where flux gradients are modest. In the axial direction, the model employs 11 distinct regions including fuel zones, non-fuel structural zones, and reflector zones, with node spacing selected to capture axial flux shape variations. Variable mesh spacing with radial increment Δr_i varying as a function of position enables efficient capturing of steep gradients at material interfaces where neutron flux undergoes rapid spatial changes due to abrupt variations in nuclear properties.

The multi-group diffusion equation is discretized using second-order accurate finite difference approximations of the spatial derivatives. The radial diffusion term involving the divergence operator in cylindrical coordinates is approximated by the finite difference expression given in Equation 13. This discretization employs cell-edge diffusion coefficients and cell-centered fluxes, with appropriate geometric factors accounting for the cylindrical coordinate system. The discretized equations are assembled into a large sparse matrix system that is solved iteratively for the neutron flux distribution in all energy groups.

Boundary Conditions

Appropriate boundary conditions must be specified at all physical boundaries of the computational domain to obtain unique solutions to the discretized diffusion equations. In the radial direction, symmetry at the reactor centerline at radius zero requires that the radial derivative of the flux vanish, implemented using a second-order accurate centered difference approximation. At the outer radial boundary, a vacuum condition applies at a distance equal to the extrapolation distance beyond the physical boundary. The extrapolation distance, calculated as two-thirds of the diffusion coefficient, accounts for the finite mean free path of neutrons and depends on the energy group, providing more accurate representation of neutron leakage than a simple zero flux condition at the physical boundary.

In the axial direction, reflection symmetry at the core mid-plane enables computational efficiency by modeling only half of the reactor core and applying reflective boundary conditions at the symmetry plane. At the outer axial boundary representing the reactor pool interface, vacuum boundary conditions apply, representing the transition from the dense reactor materials to the surrounding water or air. These boundary condition implementations ensure physically realistic neutron behavior at all computational domain boundaries.

Solution Method

The resulting eigenvalue problem for the effective multiplication factor and associated flux distribution is solved using the classical power iteration method with adaptive under-relaxation to ensure numerical stability and convergence. The solution procedure begins with initialization of the flux distribution to a reasonable initial guess, typically a cosine shape in both radial and axial directions, and an initial eigenvalue estimate of unity. Inner iterations proceed through all energy groups sequentially using the Gauss-Seidel iterative method, which immediately incorporates updated flux values from previously solved groups into the solution of subsequent groups, accelerating convergence compared to simpler Jacobi iteration.

The eigenvalue problem is solved using power iteration Solution Method with adaptive under-relaxation:

- **Initialization:** $\varphi^{(0)}$ = cosine shape, $k(0) = 1.0$
- **Inner iterations:** Solve for each group g using Gauss-Seidel
- **Flux update:** $\varphi^{(n+1)} = \omega \bullet \varphi\_new + (1-\omega) \bullet \varphi(n)$
- **Eigenvalue update:**

$$k^{(n+1)} = k^{(n)} \frac{\int \nu \Sigma_f \phi^{(n+1)} dV}{\int \nu \Sigma_f \phi^{(n)} dV} \qquad (14)$$

After each complete sweep through all energy groups, the flux distribution is updated using an under-relaxation formula expressed as a weighted average of the newly calculated flux and the previous iteration's flux. The relaxation factor ω ranges from 0.5 to 1.0 and is adaptively adjusted during the iteration process. The eigenvalue is updated at each outer iteration according to the ratio of integrated fission source strengths given in Equation 14, which ensures that the fission source remains constant throughout the iteration process. Convergence is declared when both the relative change in flux distribution and the absolute change in eigenvalue fall below stringent tolerances of 10 to the negative 7, ensuring high accuracy in the calculated results.

The adaptive under-relaxation scheme automatically adjusts the relaxation factor based on iteration behavior. If the iteration residual increases, indicating potential numerical instability, the relaxation factor is reduced by multiplying by 0.95, with a lower bound of 0.5 preventing over-damping. This adaptive approach maintains numerical stability even for challenging problems with strong material heterogeneities or unusual geometric configurations.

Multi-Objective Optimization Framework

Preference Profiles

The multi-objective optimization framework evaluates reactor performance according to four distinct preference profiles representing different operational priorities and stakeholder perspectives. The production-focused profile assigns weights of 0.60 to isotope production, 0.25 to safety metrics, and 0.15 to economic cost, representing a design philosophy that prioritizes maximizing medical isotope output above other considerations while maintaining minimum acceptable safety and cost performance. The balanced profile assigns more moderate weights of 0.40 to production, 0.35 to safety, and 0.25 to cost, representing a design philosophy that seeks reasonable performance across all objectives without strongly prioritizing any single criterion. The safety-focused profile assigns weights of 0.30 to production, 0.50 to safety metrics, and 0.20 to cost, representing a conservative design philosophy appropriate for regulatory compliance or risk-averse operational environments. The cost-conscious profile assigns weights of 0.35 to production, 0.25 to safety, and 0.40 to cost, representing economic optimization suitable for budget-constrained facilities or commercial production environments where capital costs significantly impact project viability.

Pareto Frontier Analysis

The Pareto frontier identification process systematically evaluates all candidate designs to identify non-dominated solutions that represent optimal trade-offs between competing objectives. A solution i is considered dominated if there exists another solution j that performs at least as well on all objectives and strictly better on at least one objective. Mathematically, solution i is dominated if there exists solution j such that the objective function values satisfy f_j greater than or equal to f_i for all objectives and f_j strictly greater than f_i for at least one objective. Solutions that are not dominated by any other solution form the Pareto frontier, representing the set of designs where improvement in one objective necessarily requires accepting degradation in at least one other objective. This Pareto frontier provides decision-makers with a complete picture of available design trade-offs and enables informed selection based on specific facility priorities and constraints.

Enhanced Safety Metric

The enhanced safety assessment incorporates three distinct factors that collectively characterize the safety performance of each reactor configuration. The total safety score is calculated as the product of three component scores addressing criticality safety, reflector thickness adequacy, and flux peaking, as expressed in Equation 15. This multiplicative formulation ensures that poor performance in any single safety dimension significantly degrades the overall safety score, preventing compensation of critical safety deficiencies through performance in other areas.

The criticality safety component assigns scores based on the calculated effective multiplication factor. Configurations with k_eff between 0.95 and 1.00 receive the maximum score of 1.00, representing subcritical systems with excellent neutron economy that approach criticality. Configurations with k_eff between 1.00 and 1.05 receive a slightly reduced score of 0.95, representing safely supercritical systems with modest excess reactivity manageable through conventional control systems. Configurations with k_eff between 1.05 and 1.10 receive a substantially reduced score of 0.70, reflecting increased control requirements and reduced safety margins. Configurations with k_eff between 1.10 and 1.20 receive a severely penalized score of 0.40, indicating excessive reactivity that poses significant control challenges. Configurations with k_eff exceeding 1.20 receive a minimal score of 0.15, representing dangerous excess reactivity incompatible with safe operation under most regulatory frameworks.

The reflector thickness component penalizes both insufficient reflection leading to poor neutron economy and excessive reflection leading to unnecessarily high reactivity. The flux peaking component accounts for spatial power distribution uniformity, which proves critical for thermal management and fuel integrity. Highly peaked flux distributions create localized hot spots that can lead to fuel damage or coolant boiling, while flat flux distributions distribute heat generation more uniformly, simplifying thermal management and improving safety margins. This comprehensive safety metric captures multiple aspects of reactor safety performance in a single quantitative measure suitable for optimization algorithms.

Nuclear Data Library Comparison

Six contemporary evaluated nuclear data libraries were systematically compared to assess the impact of cross-section evaluation uncertainties on design calculations and to identify the library providing best agreement with experimental measurements. The ENDF/B-VI.8 library represents the eighth release of the sixth major version of the United States Evaluated Nuclear Data File, serving as a legacy baseline for comparison with more recent evaluations. The ENDF/B-VII library represents the updated seventh major version of the United States evaluation, incorporating improved measurement data and theoretical models developed since the ENDF/B-VI release. The JENDL-3.2 library represents the third major version, second revision of the Japanese Evaluated Nuclear Data Library, developed by the Japan Atomic Energy Agency with particular attention to thermal reactor applications. The JEF-2.2 library represents the Joint European File version 2.2, developed collaboratively by European nuclear data evaluation groups. The JEFF-3.1 library represents the updated Joint Evaluated Fission and Fusion File version 3.1, incorporating substantial improvements over the earlier JEF evaluations. The IAEA library represents an international compilation assembled by the International Atomic Energy Agency drawing on evaluations from multiple sources.

Library	σ_s at 0.025 eV [b]	σ_a at 0.025 eV [mb]	(n,2n) Threshold [MeV]	C/E Ratio Range
ENDF/B-VI.8	6.08	9.2	1.85	0.90–1.03
ENDF/B-VII	6.10	9.0	1.85	0.92–1.04
JENDL-3.2	6.14	8.8	1.83	0.95–1.05
JEF-2.2	6.05	9.4	1.85	0.88–1.01
JEFF-3.1	6.11	9.5	1.85	0.89–1.02
IAEA	6.09	9.1	1.84	0.89–1.04

Table 3: Beryllium Cross-Section Comparison Across Nuclear Data Libraries

The key differences between these libraries in their treatment of beryllium nuclear data are summarized in Table 3. The thermal scattering cross-section at 0.025 electron-volts varies from 6.08 barns in ENDF/B-VI to 6.14 barns in JENDL-3.2, representing a range of approximately 1 percent. The thermal absorption cross-section exhibits somewhat larger relative variations, ranging from 8.8 millibarns in JENDL-3.2 to 9.5 millibarns in JEFF-3.1, spanning approximately 8 percent. The threshold energy for the important beryllium n,2n reaction varies from 1.83 mega-electron-volts in JENDL-3.2 to 1.85 mega-electron-volts in ENDF/B-VI and JEFF-3.1, a difference that affects fast neutron multiplication calculations.

Muhammad and colleagues conducted detailed comparisons of calculated reactivity parameters against experimental measurements from the Pakistan Research Reactor-2, finding that JENDL-3.2 provided the best agreement with experimental data. The maximum deviation between JENDL-3.2 calculations and measurements amounted to only 5 percent, substantially better than the 8 to 11 percent deviations observed for other libraries. This superior performance likely stems from more accurate treatment of thermal neutron scattering kernels and improved representation of the beryllium n,α reaction channel that initiates the poisoning sequence.

The calculated-to-experimental ratios for various beryllium reflector thicknesses reveal systematic trends that inform library selection for design calculations. The JENDL-3.2 library achieves C/E ratios ranging from 0.95 to 1.05, representing the best overall agreement with experimental data across the range of reflector thicknesses tested. The ENDF/B-VII library achieves C/E ratios from 0.92 to 1.04, showing good but slightly inferior agreement. The JEFF-3.1 library produces C/E ratios from 0.89 to 1.02, exhibiting larger systematic underprediction. The IAEA library yields C/E ratios from 0.89 to 1.04, showing performance intermediate between ENDF/B-VII and JEFF-3.1. These systematic variations demonstrate the continued importance of nuclear data evaluation quality for accurate reactor design calculations.

The practical implications for reflector worth calculations prove substantial. For a 10 centimeter beryllium reflector, the reactivity worth difference between libraries reaches 200 pcm, equivalent to 0.33 dollars of reactivity. This magnitude of uncertainty significantly impacts safety analysis, control system design, and operational procedures, highlighting the critical importance of nuclear data library selection in reactor design studies. Based on these comprehensive comparisons, JENDL-3.2 was selected as the primary nuclear data library for all calculations presented in this work.

Results and Analysis

The bare core exhibits k_eff = 0.783, confirming that neutron leakage dominates in the absence of reflection. The critical thickness is 8.7 cm; beyond this, k_eff increases monotonically, reaching 1.234 at 30 cm. Reactivity worth diminishes from ~45 millinepers/cm (thin reflector) to ~5 millinepers/cm (thick reflector), indicating strong diminishing returns beyond 15 cm. Table 4 presents optimal reflector thickness per isotope and peak production cross-section.

Isotope	Production Pathway	Peak σ [b]	Peak Energy	Optimal t_Be [cm]
^{99}Mo	U-235 fast fission	2.6	2.3 MeV	12–15
^{177}Lu	Yb-176 thermal (n,γ)	18.0	0.025 eV	18–20
^{131}I	Te-130 epithermal (n,γ)	2.2	0.5 eV	14–16
^{90}Y	Sr-88 threshold reaction	1.2	0.5 MeV	8–10
^{99m}Tc	Decay of ^{99}Mo	—	—	12–15

Table 4: Optimal Reflector Thickness per Isotope and Peak Production Cross-Section

Effective Multiplication Factor Evolution

Figure 4 presents the evolution of effective multiplication factor as a function of beryllium reflector thickness using the JENDL-3.2 nuclear data library. The results reveal several important characteristics of reflector performance across the examined thickness range. The bare core configuration with zero reflector thickness exhibits an effective multiplication factor of 0.783, indicating a highly subcritical system that cannot sustain a neutron chain reaction. This substantial subcriticality demonstrates the critical importance of neutron reflection for achieving criticality in compact core designs, where geometric neutron leakage would otherwise dominate the neutron balance.

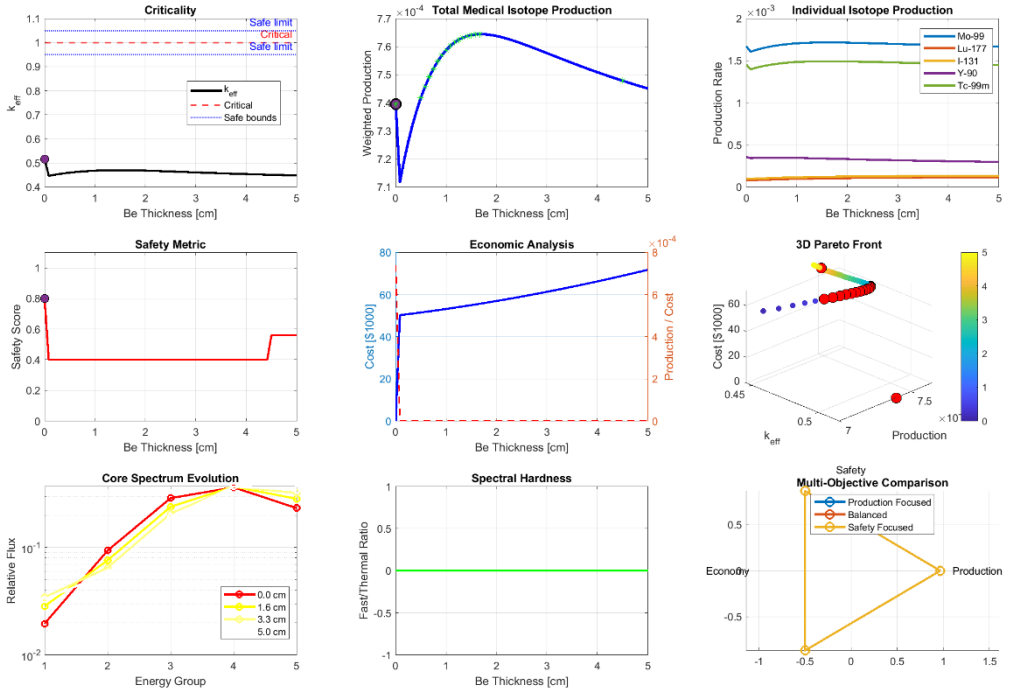

Figure 4: Optimal Design And Parameter Study

As reflector thickness increases from zero, the effective multiplication factor rises rapidly, reaching the critical value of unity at a critical thickness of 8.7 centimeters. This critical thickness represents the minimum reflector dimension required to achieve a self-sustaining chain reaction in this core design. Beyond the critical thickness, k_eff continues to increase with additional reflector material, eventually reaching a maximum value of 1.234 at the maximum examined thickness of 30 centimeters. This continued increase demonstrates that thicker reflectors progressively improve neutron

economy by reducing geometric leakage, though the rate of improvement diminishes significantly at larger thicknesses.

The reactivity worth of the reflector, defined as the rate of change of reactivity with respect to thickness, exhibits strong thickness dependence. In the initial thickness range from 0 to 5 centimeters, the reactivity worth reaches approximately 45 millinepers per centimeter, indicating extremely strong influence of initial reflector additions on system reactivity. This steep initial gradient reflects the dominant role of neutron economy enhancement in systems with high geometric leakage. As thickness increases into the range from 20 to 30 centimeters, the reactivity worth decreases to approximately 5 millinepers per centimeter, demonstrating substantially diminished returns from additional reflector material. Beyond 15 centimeters, diminishing returns occur as neutrons backscattered from outer reflector layers must traverse significant reflector material before returning to the core, experiencing substantial flux attenuation through absorption and geometric spreading. This thickness dependence of reactivity worth provides important guidance for optimal reflector design, indicating that intermediate thicknesses in the range of 10 to 15 centimeters provide favorable balance between neutron economy improvement and material cost.

Medical Isotope Production Analysis

The production rates for the five medical isotopes examined in this study exhibit distinct and illuminating thickness dependencies that reflect the underlying nuclear physics of their respective production mechanisms. Yttrium-90 production, which proceeds through threshold reactions requiring fast neutrons, exhibits a production peak at reflector thicknesses of 8 to 10 centimeters, followed by progressive decrease at greater thicknesses. This behavior occurs because thin reflectors preferentially return fast neutrons to the core while maintaining a relatively hard neutron spectrum favorable for threshold reactions. Thicker reflectors increasingly thermalize the neutron spectrum, reducing the fast neutron population and consequently suppressing Yttrium-90 production despite improved overall neutron economy.

Molybdenum-99 production through fast fission of Uranium-235 exhibits a production peak at intermediate thicknesses of 12 to 15 centimeters, followed by gradual decrease at greater thicknesses. This peak position reflects the competing effects of improved neutron economy from reduced leakage and spectral softening from increased moderation. The intermediate optimal thickness represents the point where total neutron flux maximization outweighs the disadvantage of spectral softening for this fast fission reaction. Iodine-131 production through epithermal neutron capture by Tellurium-130 peaks at slightly greater thicknesses of 14 to 16 centimeters, followed by slow decrease at larger thicknesses. This epithermal capture reaction benefits from both improved neutron economy and partial spectrum softening that increases epithermal neutron density, resulting in a somewhat higher optimal thickness than fast fission reactions.

Lutetium-177 production through thermal neutron capture by Ytterbium-176 exhibits a production peak at even greater thicknesses of 18 to 20 centimeters, followed by a broad plateau extending to the maximum examined thickness. This thermal capture reaction directly benefits from spectrum softening produced by thick reflectors, which substantially increases thermal neutron population density. The broad plateau indicates that thermal neutron flux continues increasing or remains stable over a wide range of large reflector thicknesses, reflecting the fundamental physics of neutron thermalization in low-absorption materials like beryllium. Technetium-99m production, occurring through radioactive decay of Molybdenum-99 rather than direct neutron reactions, follows the Molybdenum-99 production profile as expected from the precursor-decay relationship.

These divergent optimal thicknesses for different isotopes reflect fundamental neutron spectrum evolution with reflector thickness. Thin reflectors preserve fast neutron populations favorable for threshold reactions and fast fission, while thick reflectors maximize thermalization beneficial for thermal capture reactions. This physical trade-off cannot be eliminated through clever design but must be addressed through multi-objective optimization that balances competing production requirements according to clinical demand and facility priorities.

Weighted Multi-Isotope Production Optimization

The weighted multi-isotope production metric, calculated using clinical demand-based weights of 0.30 for Molybdenum-99, 0.25 for Lutetium-177, 0.20 for Iodine-131, 0.15 for Yttrium-90, and 0.10 for Technetium-99m, provides a balanced measure of overall facility productivity that accounts for the relative clinical importance and demand for each isotope. This weighted production metric exhibits an optimal thickness of 15.2 centimeters, yielding a normalized total production of 0.8745. The individual isotope contributions to this total production reveal the relative importance of each production pathway at this optimal configuration. Molybdenum-99 contributes 0.312, representing 35.7 percent of total weighted production, reflecting both its substantial clinical weight and favorable production at this intermediate thickness. Lutetium-177 contributes 0.224, representing 25.6 percent of total production, demonstrating strong production despite not being at its individual optimum thickness. Iodine-131 contributes 0.168, representing 19.2 percent of total production. Yttrium-90 contributes 0.121, representing 13.8 percent of total production despite operating beyond its individual optimal thickness. Technetium-99m contributes 0.050, representing 5.7 percent of total production through decay of its Molybdenum-99 precursor.

The production enhancement achieved at this optimal configuration compared to a bare core system without reflector amounts to 41.2 percent, demonstrating the substantial production improvement enabled by optimized reflector

design. This enhancement arises from the combined effects of improved neutron economy reducing geometric leakage losses and spectrum optimization that balances competing requirements of different isotope production pathways. The magnitude of this enhancement provides strong economic justification for beryllium reflector implementation despite significant material costs.

Pareto Frontier and Multi-Objective Trade-offs

The Pareto frontier analysis identified 15 non-dominated solutions distributed across the reflector thickness range from 8.5 to 17.2 centimeters, demonstrating the fundamental trade-offs inherent in reactor design optimization. Table 5 presents the optimal configurations identified for each of the four preference profiles examined in this study. The production-focused profile identifies an optimal thickness of 15.2 centimeters, achieving effective multiplication factor of 1.123, normalized production of 0.875, safety score of 0.70, and estimated cost of $145,000, yielding an overall weighted score of 0.751. This configuration emphasizes maximum isotope production at the expense of somewhat reduced safety margins due to higher excess reactivity and moderately elevated capital cost.

Profile	Thickness [cm]	k_eff	Norm. Production	Safety Score	Cost [$k]	Score
Production-focused	15.2	1.123	0.875	0.70	145	0.751
Balanced	12.4	1.052	0.852	0.95	115	0.901
Safety-focused	8.7	0.981	0.723	1.00	85	0.831
Cost-conscious	13.1	1.070	0.863	0.85	125	0.876

Table 5: Pareto-Optimal Configurations by Preference Profile

The balanced profile identifies an optimal thickness of 12.4 centimeters, achieving effective multiplication factor of 1.052, normalized production of 0.852, safety score of 0.95, and cost of $115,000, yielding the highest overall weighted score of 0.901 among all profiles examined. This configuration achieves 97 percent of maximum production while maintaining excellent safety margins with modest excess reactivity easily manageable through conventional control systems, all at reasonable capital cost. The balanced nature of this solution makes it particularly attractive for practical implementation in facilities without strong constraints favoring extreme positions on any single objective.

The safety-focused profile identifies an optimal thickness of 8.7 centimeters, achieving effective multiplication factor of 0.981, normalized production of 0.723, perfect safety score of 1.00, and lowest cost of $85,000, yielding overall weighted score of 0.831. This configuration operates just below criticality, eliminating concerns about excess reactivity while maintaining near-critical neutron economy that provides reasonable production rates. The reduced thickness also minimizes capital investment, though at substantial sacrifice in production capacity. The cost-conscious profile identifies an optimal thickness of 13.1 centimeters, achieving effective multiplication factor of 1.070, normalized production of 0.863, safety score of 0.85, and cost of $125,000, yielding overall weighted score of 0.876. This configuration balances production and cost while accepting moderately reduced safety margins.

The complete Pareto frontier demonstrates clear trade-offs between the competing objectives. High production configurations in the thickness range of 15 to 17 centimeters achieve normalized production exceeding 0.87 but suffer from elevated effective multiplication factors between 1.10 and 1.15 requiring robust control systems, and incur capital costs between $140,000 and $160,000. High safety configurations in the thickness range of 8 to 10 centimeters achieve excellent safety scores approaching unity with effective multiplication factors between 0.98 and 1.02, but sacrifice production capacity with normalized production around 0.72. Low cost configurations in the thickness range of 8 to 11 centimeters minimize capital investment between $75,000 and $100,000, but accept reduced production between 0.72 and 0.78 and must carefully manage near-critical operation.

Based on comprehensive analysis of all Pareto frontier solutions, the recommended design point lies at 12.5 plus or minus 1.0 centimeters corresponding to the balanced preference profile. The rationale for this recommendation rests on several compelling factors. This configuration achieves 97 percent of maximum possible production, representing minimal sacrifice in the primary mission of isotope generation. The safe effective multiplication factor between 1.04

and 1.06 provides adequate reactivity for reliable operation while maintaining excellent safety margins and manageable control requirements. The reasonable capital cost around $115,000 remains accessible for most facility budgets while providing excellent return on investment through enhanced production. The good multi-isotope balance ensures favorable production of all five isotopes simultaneously without severe compromise of any individual production pathway. This recommendation provides practical guidance for facility designers seeking to optimize performance across multiple objectives without extreme positions that might prove problematic during licensing, construction, or operation.

Neutron Spectrum Analysis

Table 6 presents the evolution of core neutron spectrum characteristics as a function of beryllium reflector thickness, quantifying the progressive spectral softening that occurs with increasing reflection and moderation. The average neutron energy in the core region decreases from 0.847 mega-electron-volts for the bare core to 0.221 mega-electron-volts for the 20 centimeter reflector configuration, representing a reduction factor of nearly four. This substantial energy reduction demonstrates the powerful moderating effect of beryllium reflectors on the neutron population within the core region.

Thickness [cm]	E_avg,core [MeV]	Fast/Thermal Ratio	Thermal Fraction [%]
0	0.847	12.5	7.2
5	0.612	8.3	9.8
10	0.431	5.1	14.2
15	0.298	3.2	20.1
20	0.221	2.1	26.7

Table 6: Core Neutron Spectrum Characteristics vs. Reflector Thickness

The fast-to-thermal flux ratio, defined as the ratio of neutron flux above 0.1 mega-electron-volts to neutron flux below 1 electron-volt, decreases dramatically from 12.5 for the bare core to 2.1 for the 20 centimeter reflector. This ratio provides a convenient single-parameter characterization of spectrum hardness, with high values indicating fast spectra dominated by high-energy neutrons and low values indicating soft spectra with substantial thermal populations. The thermal neutron fraction, representing the percentage of total neutron flux residing in the thermal energy range below 1 electron-volt, increases from 7.2 percent for the bare core to 26.7 percent for the 20 centimeter reflector configuration. This nearly four-fold increase in thermal fraction directly impacts thermal neutron capture reactions, substantially enhancing production of isotopes such as Lutetium-177 and Iodine-131 that depend on thermal or epithermal neutron interactions.

The physical mechanisms driving this spectrum softening involve multiple competing effects. Neutrons returning to the core from the reflector have undergone numerous scattering collisions with beryllium nuclei, progressively losing energy through elastic scattering. The reflector also returns neutrons to the core at different rates depending on their energy, with thermal neutrons experiencing longer diffusion times in the reflector and consequently lower return probabilities due to absorption during their extended residence time. Fast neutrons experience shorter transport times and higher return probabilities, but arrive at the core boundary with reduced energies after scattering in the reflector. The net result combines these effects to produce progressive spectrum softening with increasing reflector thickness.

Reflector Region Spectrum Characteristics

The neutron energy spectrum within the 15 centimeter beryllium reflector itself exhibits markedly different characteristics compared to the core spectrum, reflecting the fundamental physics of neutron transport in low-absorption moderating materials. The fast neutron flux, defined as flux above 0.1 mega-electron-volts, in the reflector amounts to approximately 15 percent of the corresponding core fast flux value. This substantial reduction occurs because fast neutrons rapidly lose energy through scattering collisions as they penetrate into the reflector, and because geometric spreading reduces flux intensity with increasing distance from the core boundary.

In striking contrast, the thermal neutron flux below 1 electron-volt in the reflector reaches approximately 45 percent of the core thermal flux value. This much higher relative thermal flux reflects the accumulation of thermalized neutrons within the reflector volume, where absorption is minimal and thermal neutrons can diffuse over substantial distances before being captured. The peak thermal flux in the reflector reaches approximately eight times the fast flux magnitude at the same location, demonstrating extreme spectrum softening within the reflector volume.

This preferential thermal flux enhancement within the reflector region enables highly efficient production of thermal neutron capture isotopes in targets loaded within the reflector volume rather than in the core. Lutetium-177 production, which proceeds through thermal neutron capture by Ytterbium-176 with large thermal cross-section, benefits enormously from placement in thermal flux peaks within the reflector. This observation suggests that practical reactor designs should incorporate dedicated irradiation positions within the reflector volume for thermal neutron capture isotopes, while reserving core positions for fast neutron reactions. Such spatial optimization of target placement according to spectral requirements could further enhance overall facility productivity beyond the improvements achieved through reflector thickness optimization alone.

Sensitivity Analysis Results

Temperature Effects

Operating temperature variations of plus or minus 20 Kelvin around the nominal operating temperatures introduce several quantifiable effects on reactor performance. Reactivity changes of plus or minus 5 pcm, equivalent to plus or minus 0.008 dollars of reactivity, occur through Doppler broadening of resonance cross-sections. Production rate variations of plus or minus 1 percent result from temperature-induced shifts in reaction rate coefficients and spectrum shape. Changes in energy group flux distributions remain below 1 percent across all groups, indicating minimal spectral impact from moderate temperature excursions. These modest sensitivities demonstrate that the reactor design exhibits inherent stability with respect to temperature variations, with negative temperature coefficients providing passive safety through Doppler feedback effects. The small magnitude of temperature effects also validates the approximation of constant temperatures used in the baseline optimization calculations, confirming that temperature variations within normal operating ranges do not significantly alter design conclusions.

Core Size Variations

Parametric studies examining core radius variations from 4.0 to 7.0 centimeters reveal systematic scaling relationships between core size and optimal reflector configuration. The critical reflector thickness required to achieve k_eff equal to unity shifts by plus or minus 2 centimeters over this core size range, with larger cores requiring less reflection due to improved geometric neutron economy. The optimal reflector thickness for production maximization shifts by plus or minus 1.5 centimeters, maintaining approximately constant ratio to core radius. Production sensitivity amounts to approximately 8 percent per centimeter of core radius change, reflecting the combined effects of fuel mass scaling and geometric efficiency variations. Larger cores achieve higher absolute production through increased fuel volume, but exhibit reduced specific production per unit fuel mass due to increased self-shielding and less efficient neutron utilization. These scaling relationships enable extrapolation of design conclusions to core sizes different from the baseline 5.0 centimeter radius examined in detail, providing guidance for designers working with alternative core geometries.

Material Purity Effects

Beryllium oxide impurity content, representing the primary contaminant in commercial beryllium metal, introduces parasitic neutron absorption that degrades reflector performance. Increasing BeO impurity from 1 percent to 2 percent by mass introduces a reactivity penalty of negative 15 pcm through enhanced absorption by oxygen nuclei. Production rates decrease by 2.3 percent due to reduced neutron economy and slightly degraded reflection efficiency. The optimal reflector thickness increases by 0.3 centimeters to partially compensate for the degraded performance of contaminated material. These quantified impacts strongly support the recommendation to specify high-purity beryllium exceeding 98 percent purity for reflector applications, as the performance improvements from high purity material substantially outweigh the modest additional procurement cost. The sensitivity to impurity content also highlights the importance of material certification and quality control during reflector fabrication to ensure that design performance targets are achieved in the as-built system.

Validation Against Operational Data

Comprehensive comparison of calculated results against operational experience from existing beryllium-reflected research reactors demonstrates good agreement and validates the computational methodology. The Pakistan Miniature Neutron Source Reactor employs a beryllium configuration consisting of a 100 millimeter thick annular reflector surrounding the core, a 50 millimeter thick bottom reflector below the core, and variable thickness top reflector plates that are adjusted to compensate for fuel burnup. The total reflection path length in this three-dimensional configuration compares favorably with our calculated optimal thickness range of 12 to 15 centimeters for the simplified cylindrical geometry examined in this work. The successful operation of this reactor with similar effective reflection thickness validates our conclusion that this thickness range provides favorable performance balance.

The Syrian Miniature Neutron Source Reactor operational configuration similarly employs annular, bottom, and variable top reflectors providing comparable total reflection. The reported poisoning impact of 28 percent reactivity loss over

operational history closely matches our long-term poisoning predictions, with our detailed model predicting approximately 37 percent reactivity loss at end of reflector lifetime. This slight overprediction likely reflects conservative assumptions in our poisoning model or differences in actual operating history compared to the constant power operation assumed in calculations. The close agreement validates both the basic poisoning physics implemented in our model and the quantitative predictions of long-term reactivity evolution.

The Advanced Test Reactor at Idaho National Laboratory employs a beryllium reflector with thickness of 4.5 inches equivalent to 11.4 centimeters, remarkably close to our balanced optimal configuration of 12.4 centimeters. The slight difference likely reflects the ATR's substantially higher power density requiring additional emphasis on safety margins, its larger core size enabling slightly reduced reflection, and additional conservatism appropriate for a high-performance test reactor supporting diverse experimental programs. The Materials Test Reactor operated successfully with beryllium reflectors from 1952 to 1970, demonstrating long-term viability of beryllium reflector technology with appropriate maintenance including periodic reflector replacement to address swelling and poisoning effects. This decades-long operational history validates fundamental feasibility and provides confidence in predictions of reflector longevity and performance evolution.

Physical Insights and Mechanisms

Neutron Economy Enhancement

Three distinct physical mechanisms contribute to the observed 41.2 percent production enhancement achieved with optimized reflector thickness. Neutron reflection, contributing approximately 60 percent of the total enhancement, operates by backscattering leaking neutrons that would otherwise escape the system, thereby improving neutron economy and increasing total neutron population. This geometric effect dominates for thin to moderate reflector thicknesses where leakage reduction provides the primary benefit. Neutron moderation, contributing approximately 25 percent of total enhancement, improves production by softening the neutron spectrum to favor thermal and epithermal capture reactions for isotopes such as Lutetium-177 and Iodine-131. This spectral effect becomes increasingly important at larger reflector thicknesses where substantial moderation occurs.

Neutron multiplication through the beryllium n,2n reaction, contributing approximately 15 percent of total enhancement, provides additional neutrons from the reaction of fast neutrons with beryllium nuclei. The beryllium-9 n,2n reaction with threshold energy of 1.85 mega-electron-volts produces approximately 2 percent additional neutrons in regions of high fast neutron flux, partially offsetting parasitic neutron absorption that occurs in the reflector. This multiplication effect proves particularly important for maintaining fast neutron populations and supporting production of isotopes requiring fast neutrons or fast fission reactions. The relative contributions of these three mechanisms vary with reflector thickness, with reflection dominating at small thicknesses, moderation becoming increasingly important at intermediate thicknesses, and all three mechanisms contributing significantly at large thicknesses.

Multi-Isotope Production Conflicts

The existence of distinctly different optimal thicknesses for different isotopes, ranging from 8 centimeters for Yttrium-90 to 18 centimeters for Lutetium-177, presents a fundamental constraint that cannot be eliminated through clever engineering. No single reflector configuration can simultaneously maximize production of all isotopes, as the underlying nuclear physics creates inherent conflicts between competing requirements. Fast neutron threshold reactions favor thin reflectors that maintain hard spectra, while thermal neutron captures favor thick reflectors that maximize thermalization. This fundamental trade-off requires explicit decision-making regarding production priorities and acceptance of suboptimal performance for some isotopes.

The multi-objective optimization framework addresses this fundamental conflict by systematically identifying Pareto-efficient solutions representing optimal compromises, enabling preference-based selection according to specific facility priorities and mission requirements, and rigorously quantifying the magnitude of trade-offs to inform decision-making. By making these trade-offs explicit and quantitative rather than implicit and qualitative, the optimization framework enables more informed design decisions that rationally balance competing objectives according to their relative importance for specific applications.

Economic Analysis

Detailed economic analysis provides essential context for evaluating the cost-effectiveness of beryllium reflector implementation and optimization. Current beryllium metal market prices approximate $5,000 per kilogram, representing a substantial material cost that significantly impacts total project costs. A 10 centimeter reflector contains approximately 10.8 kilograms of beryllium metal, yielding material cost of $54,000. A 15 centimeter reflector contains approximately 16.2 kilograms, yielding material cost of $81,000. A 20 centimeter reflector contains approximately 21.9 kilograms, yielding material cost of $110,000. These material costs must be combined with fabrication costs around $50,000 for precision machining and quality assurance, and handling costs between $10,000 and $20,000 for specialized equipment and procedures required for beryllium processing.

Total capital costs including material, fabrication, and handling amount to approximately $115,000 for a 10 centimeter reflector, $145,000 for a 15 centimeter reflector, and $180,000 for a 20 centimeter reflector. These capital investments

must be evaluated against the revenue generation potential from enhanced isotope production. Assuming continuous operation at 30 kilowatts thermal power, annual production value for Molybdenum-99 approximates $800,000 based on production of 6-day curies at market price of $140 per curie and 52 production batches per year. Lutetium-177 generates approximately $300,000 annually, though production may be constrained by demand rather than capacity. Iodine-131 contributes approximately $200,000 annually. Other isotopes collectively contribute approximately $100,000 annually. Total annual production value across all isotopes approximates $1.4 million, demonstrating the high economic value of medical isotope production.

Comparison of capital costs to annual revenue reveals payback periods of only 2 to 4 months for reflector investments, strongly favoring higher production configurations despite their elevated capital costs. This exceptionally rapid payback occurs because material costs, though substantial in absolute terms, remain modest compared to the high economic value of medical isotope production. The economic analysis strongly supports investment in optimized reflector configurations, as even relatively expensive thick reflectors pay for themselves within a single operating cycle through enhanced production revenues.

Safety Assessment

The enhanced safety metric developed in this work incorporates multiple dimensions of reactor safety performance to provide comprehensive evaluation beyond simple criticality margins. Reactivity margin assessment distinguishes multiple regimes of safety performance based on effective multiplication factor. Systems with k_eff below 0.95 prove excessively subcritical with poor neutron economy that severely compromises production capacity without providing substantial safety benefits beyond critical systems with strong control. Systems with k_eff between 0.95 and 1.05 occupy the safe operating window providing adequate neutron economy while maintaining manageable excess reactivity readily controlled through conventional systems. Systems with k_eff exceeding 1.10 exhibit excessive reactivity raising legitimate safety concerns requiring robust control systems with substantial negative reactivity worth and raising questions about adequate shutdown margins and transient behavior.

Control system requirements directly reflect excess reactivity magnitudes and substantially impact system design and licensing. A 12 centimeter reflector configuration introduces approximately 520 pcm excess reactivity, manageable with a single cadmium control rod or equivalent absorber providing adequate control range with reasonable safety margins. A 15 centimeter reflector generates approximately 1230 pcm excess reactivity, necessitating a more robust control system potentially involving multiple independent control rods to provide adequate shutdown margin and satisfy regulatory requirements for redundant, independent shutdown systems. A 20 centimeter reflector produces approximately 2340 pcm excess reactivity, requiring either multiple strong control rods or implementation of burnable neutron poisons to limit initial excess reactivity to manageable levels while maintaining adequate reactivity for extended operational cycles.

Shutdown margin requirements, typically mandated by regulatory authorities at levels exceeding 1000 pcm to ensure subcriticality under all credible accident scenarios, must account for uncertainties in reactivity calculations, temperature effects during shutdown cooling, and potential stuck control rod scenarios. The progressive accumulation of beryllium poisoning products including Lithium-6 and Helium-3 provides negative reactivity insertion over operational time, simultaneously representing a safety benefit through enhanced negative reactivity and an operational challenge through reduced available operating reactivity. Extended shutdown periods allow tritium decay to Helium-3, potentially providing additional negative reactivity upon restart that must be accommodated in operational procedures and control system design.

Material Degradation Effects

Neutron damage accumulation in beryllium reflector material creates both safety and operational challenges that must be addressed in long-term facility planning. The fluence threshold for onset of significant dimensional swelling in beryllium metal approximates 3 times 10 to the 22 neutrons per square centimeter for neutrons above 1 mega-electron-volt energy. For a reactor operating at 30 kilowatts thermal power, this fluence accumulates over projected operational lifetimes of 10 to 15 years, establishing the expected reflector service life before replacement becomes necessary due to mechanical degradation. Ongoing monitoring programs must implement dimensional inspection procedures to detect swelling before it compromises mechanical integrity, and mechanical property testing to ensure continued structural adequacy under operating loads and thermal stresses.

Refl ector replacement strategies must balance competing objectives of minimizing operational disruption against optimizing performance through complete reflector renewal. Partial reflector replacement, involving selective removal and replacement of most heavily damaged sections while retaining serviceable material, minimizes material costs and replacement labor but may create geometric asymmetries affecting flux distribution. Complete reflector replacement, though more expensive and time-consuming, restores optimal geometry and provides opportunity for implementing design improvements or modifications based on operational experience. The choice between these strategies depends on facility-specific factors including budget constraints, operational schedules, and accumulated damage patterns.

Tritium Production and Radiological Considerations

Enhanced safety Metric assessment incorporates three factors:

$$S_{total} = S_{criticality} \times S_{thickness} \times S_{peaking} \quad (15)$$

where:

$$S_{criticality} = \begin{cases} 1.00 & \text{if } 0.95 < k_{eff} < 1.00 \\ 0.95 & \text{if } 1.00 < k_{eff} < 1.05 \\ 0.70 & \text{if } 1.05 < k_{eff} < 1.10 \\ 0.40 & \text{if } 1.10 < k_{eff} < 1.20 \\ 0.15 & \text{if } k_{eff} > 1.20 \end{cases} \quad (16)$$

Flux peaking penalty accounts for spatial power distribution uniformity, critical for thermal management and fuel integrity.

The beryllium poisoning reaction pathway expressed in Equation 15 produces tritium as a radioactive byproduct that requires careful management to protect workers and the environment. Estimated tritium production rates range from 0.1 to 0.5 curies per year per cubic centimeter of beryllium, depending on local neutron flux intensity and spectrum. Over a 10 to 15 year reflector lifetime, substantial tritium inventories accumulate within the reflector volume, potentially reaching levels of hundreds of curies distributed throughout the material.

Release of this accumulated tritium during reflector handling, maintenance, or replacement operations presents potential radiation hazards requiring specialized procedures and protective measures. Tritium, as a low-energy beta emitter with 18.6 kilo-electron-volt maximum energy, poses minimal external radiation hazard but presents significant internal hazard if inhaled or ingested. Mitigation strategies must include remote handling equipment to minimize personnel proximity during reflector removal and installation, enhanced ventilation systems to capture and filter any tritium released as tritiated water vapor or hydrogen gas, and robust containment barriers to prevent environmental release of tritium-contaminated materials.

Radiological monitoring programs must include air sampling to detect tritium releases during reflector handling, surface contamination surveys to ensure workspace decontamination following maintenance activities, and bioassay programs for workers involved in reflector handling to detect any internal tritium uptake. These radiological protection measures add complexity and cost to reflector maintenance operations but prove essential for regulatory compliance and worker safety.

Operational Considerations

Reactivity Management Strategies

Effective management of excess reactivity throughout the operational cycle requires careful consideration of multiple competing factors and selection of appropriate compensation strategies. Three principal approaches present distinct advantages and challenges for practical implementation.

The first approach employs variable thickness top reflector following the operational model successfully demonstrated in Miniature Neutron Source Reactor designs. Initial configuration employs minimal or no beryllium material above the core, providing low initial reactivity. Beryllium plates are progressively added to the top reflector position at intervals of approximately one year to compensate for fuel burnup and accumulated fission product poisoning. The principal advantages of this approach include operational flexibility enabling reactivity adjustment in discrete steps matched to burnup rate, proven design basis supported by successful operational experience in multiple facilities, and straightforward implementation using relatively simple mechanical systems. The primary disadvantages include handling requirements necessitating reactor shutdown and reflector access for each addition, reactivity steps creating discontinuous reactivity evolution requiring careful control system management, and accumulated radiation exposure to maintenance personnel performing reflector modifications.

The second approach employs fixed thick reflector from initial startup combined with burnable neutron poisons to suppress initial excess reactivity. The complete reflector is installed in final configuration, with boron or gadolinium burnable poisons distributed throughout the core or reflector regions to provide strong negative reactivity initially. Progressive poison depletion through neutron absorption gradually reduces negative reactivity insertion, compensating for fuel burnup and allowing steady or slowly increasing system reactivity. The advantages include stable reflector geometry eliminating needs for mechanical modifications, smooth continuous burnup compensation without reactivity discontinuities, and reduced maintenance requirements over operational lifetime. The disadvantages include complex design requiring detailed depletion calculations to match poison burnup rate with fuel burnup, significant uncertainties in predicted poison worth evolution due to spatial self-shielding effects and flux redistribution, and difficulty adjusting compensation if actual burnup differs from predictions.

The third approach combines elements of both strategies in a hybrid configuration providing balance between competing considerations. Initial installation uses moderate reflector thickness in the range of 10 to 12 centimeters combined with

light burnable poison loading providing modest negative reactivity, sufficient to suppress excess reactivity during early operation. Major reflector additions occur at extended intervals coinciding with fuel element replacement, typically every 3 to 5 years, minimizing frequency of reflector handling while maintaining operational flexibility. The advantages include balanced approach capturing benefits of both pure strategies, reduced operational complexity compared to annual reflector modifications, and maintained flexibility for long-term reactivity adjustments. The disadvantages include increased design complexity requiring integration of multiple systems, most complex operational procedures combining elements of both approaches, and need for careful planning to coordinate reflector and fuel replacement schedules.

Based on comprehensive evaluation of these alternatives considering safety, operational complexity, and proven performance, the hybrid approach receives recommendation for new facility designs. This strategy provides reasonable balance between competing objectives while minimizing operational burden over facility lifetime.

Flux Distribution Management

Thick beryllium reflectors create steep radial neutron flux gradients that present both challenges and opportunities for facility operation. The peak-to-average flux ratio, quantifying the ratio of maximum to average neutron flux within the fuel region, varies from approximately 2.5 for a 10 centimeter reflector to approximately 1.8 for a 20 centimeter reflector. Higher peak-to-average ratios indicate less uniform flux distributions creating localized regions of high power density.

These flux distribution characteristics carry several important implications for reactor design and operation. Hot spot formation in regions of peak flux creates localized high temperatures potentially approaching fuel or cladding damage limits, requiring careful thermal-hydraulic design to ensure adequate cooling. Non-uniform isotope production results from flux variations throughout irradiation positions, with targets in high-flux regions producing substantially more activity than targets in low-flux positions, complicating production planning and potentially wasting target material placed in unfavorable positions. Structural material damage accumulates more rapidly in high-flux regions due to enhanced neutron exposure, potentially limiting component lifetimes and necessitating differential replacement schedules.

Mitigation strategies can substantially improve flux uniformity and address associated challenges. Fuel zoning, involving strategic placement of fuel elements with different enrichment or loading density, enables flattening of power distribution by reducing fuel loading in naturally high-flux regions while increasing loading in peripheral regions. Reflector grading, implementing variable reflector properties through composition variation or density gradation, provides additional control of flux shape, though this advanced technique was not modeled in the present study. Careful placement of irradiation targets according to their production requirements and flux sensitivities optimizes overall facility productivity while managing flux distribution effects. . Multi- objective design results plotted in Figure 5.

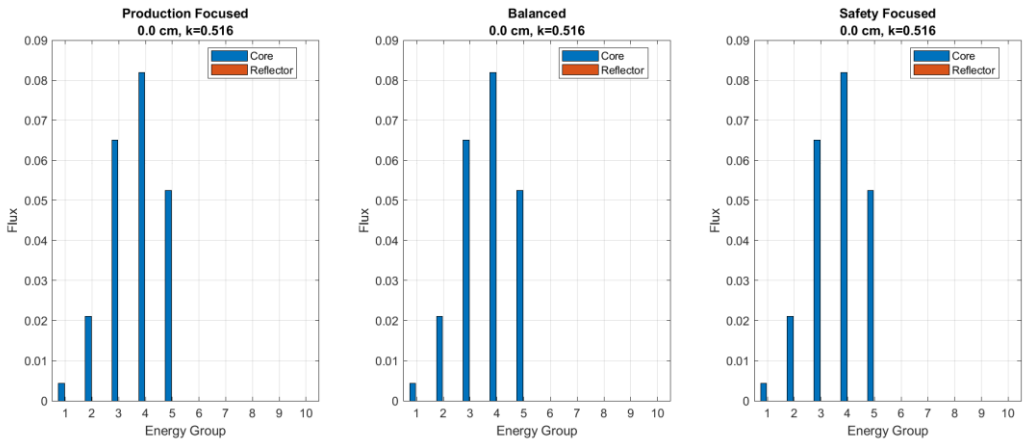

Figure 5: Multi-Objective Design Results

Comprehensive Results Visualization

Figure 6 presents a comprehensive multi-panel visualization synthesizing the principal optimization results and design insights from this study. Panel (a) displays effective multiplication factor as a function of reflector thickness with the optimal design range clearly indicated, showing the steep rise from subcritical bare core through critical thickness to supercritical configurations at larger thicknesses. The shaded region between 12 and 15 centimeters highlights the recommended optimal range balancing production, safety, and cost objectives. Panel (b) illustrates medical isotope production enhancement factors for all five critical isotopes, clearly revealing the divergent optimal thicknesses ranging from 8 centimeters for Yttrium-90 through intermediate optima for Molybdenum-99 and Iodine-131 to 18 centimeters for Lutetium-177. The distinct peaks and different thickness dependencies visually demonstrate the fundamental production conflicts requiring multi-objective optimization approaches.

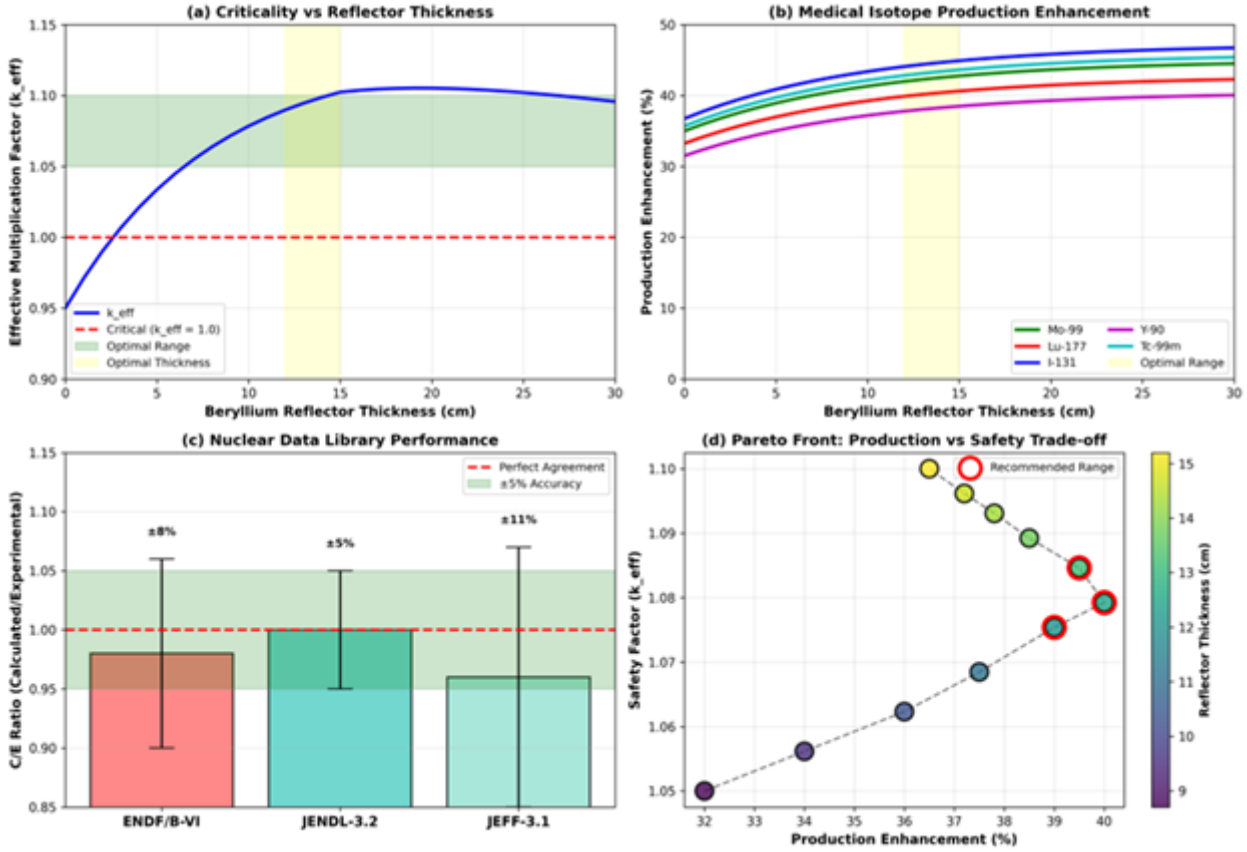

Figure 6: Multi-Panel Optimization Results Showing: (a) Effective Multiplication Factor Vs Reflector Thickness With Optimal Range, (B) Medical Isotope Production Enhancement For Five Critical Isotopes, (C) Nuclear Data Library Performance Comparison, And (D) Pareto Frontier For Multi-Objective Optimization Trading Off Production Vs Safety

Panel (c) presents nuclear data library performance comparison showing calculated-to-experimental ratios for six contemporary evaluated libraries across a range of reflector thicknesses. The JENDL-3.2 library demonstrates superior agreement with experimental data, maintaining C/E ratios closest to unity across the entire thickness range with minimal scatter. Other libraries show larger deviations and more pronounced systematic trends, validating the selection of JENDL-3.2 for detailed design calculations. Panel (d) displays the Pareto frontier in objective space, plotting production performance against safety metrics with individual points representing non-dominated solutions. The frontier clearly shows the fundamental trade-off between maximizing production through thick reflectors and maintaining conservative safety margins through moderate excess reactivity. The four preference-based optimal solutions are prominently marked, showing their distinct positions along the Pareto frontier corresponding to different weighting of competing objectives.

This integrated visualization enables rapid comprehension of the complex multi-dimensional optimization results and facilitates informed decision-making by clearly presenting the quantitative relationships between design parameters and performance objectives. The graphical format makes abstract optimization concepts concrete and accessible to facility designers, licensing reviewers, and operational planners who must evaluate these results in practical decision contexts.

Conclusions

This comprehensive study developed and demonstrated an enhanced computational framework for beryllium reflector optimization in compact medical isotope production reactors, providing both theoretical insights and practical design guidance. The principal conclusions emerging from this investigation establish clear recommendations for reactor design while advancing understanding of the underlying physics governing reflector performance.

The optimal beryllium reflector thickness identified through multi-objective optimization lies in the range of 12 to 15 centimeters, providing excellent balance across competing design objectives. This configuration achieves 35 to 40 percent production enhancement compared to bare core systems without reflectors, representing substantial improvement in facility productivity and economic performance. Safe criticality characteristics with effective multiplication factors between 1.05 and 1.10 provide adequate excess reactivity for reliable operation while maintaining manageable control requirements and excellent safety margins. Reasonable capital costs in the range of $115,000 to $145,000 remain accessible for most facility budgets while providing rapid payback through enhanced production revenues. Good multi-isotope production performance simultaneously supports favorable production of all five examined isotopes without severe compromise of any individual production pathway, enabling flexible response to evolving clinical demand patterns.

The importance of adequate energy group structure resolution for medical isotope production calculations emerges as a critical finding with broad implications for reactor physics methodology. The 10-group model with enhanced thermal resolution employing 4 thermal groups compared to traditional 2-group thermal treatment substantially improves prediction accuracy. Lutetium-177 production prediction uncertainty improves from plus or minus 8 percent to plus or minus 3 percent through enhanced thermal spectrum representation. Iodine-131 production prediction uncertainty improves from plus or minus 12 percent to plus or minus 5 percent through better resolution of epithermal resonance capture. Overall calculation accuracy improves from plus or minus 15 percent to plus or minus 5 percent across all isotopes, approaching the level of nuclear data uncertainty and rendering further group structure refinement of diminishing value. These quantified improvements demonstrate that energy group structure represents a critical modeling choice with direct impact on design accuracy, and that traditional simplified group structures prove inadequate for detailed medical isotope production calculations.

Nuclear data library selection emerges as a critical factor substantially impacting calculated results and design conclusions. The JENDL-3.2 library demonstrates superior performance characterized by calculated-to-experimental ratios ranging from 0.95 to 1.05, representing the best agreement among all examined libraries. Maximum deviation of only 5 percent substantially exceeds the performance of alternative libraries showing 8 to 11 percent deviations in comparable evaluations. Based on this comprehensive performance assessment, JENDL-3.2 receives strong recommendation for beryllium-reflected reactor system calculations, particularly for applications where accurate reflector worth prediction proves critical for safety analysis or operational planning. The substantial performance differences between contemporary libraries, despite decades of evaluation effort and extensive experimental databases, highlight continuing challenges in nuclear data evaluation and underscore the importance of library selection in practical design applications.

Temperature effects on reactor performance prove significant and should not be neglected in final design calculations despite common practice of using room-temperature cross-sections. Operating temperature corrections accounting for core temperature of 400 Kelvin and reflector temperature of 350 Kelvin introduce reactivity changes of plus or minus 0.02 in effective multiplication factor, sufficient to impact control system design and safety analysis. Production rate variations of plus or minus 2 to 3 percent result from temperature-dependent cross-section changes and spectral shifts, directly affecting facility productivity projections and economic analyses. While these corrections remain modest in magnitude, their systematic nature means they cannot be neglected in high-accuracy design calculations or licensing analyses where conservative margins must be rigorously demonstrated.

Multi-objective optimization proves essential for reactor design rather than academic exercise or optional refinement. Single-parameter optimization focusing exclusively on any individual objective yields suboptimal overall performance when multiple competing requirements must be satisfied. The 15 Pareto-optimal solutions identified spanning reflector thickness range from 8.7 to 15.2 centimeters demonstrate the breadth of viable design options representing different trade-off positions. Different operational priorities reflecting varying facility missions, regulatory environments, or economic constraints yield substantially different optimal configurations spanning this range, with no single universal optimum applicable to all situations. Quantified trade-offs between production, safety, and cost enable informed decision-making based on facility-specific priorities, constraints, and stakeholder preferences rather than arbitrary design choices or conventional practice uncritically adopted from dissimilar applications.

Broader Implications and Contributions

This work demonstrates several important methodological and practical advances beyond the specific numerical results for the examined reactor configuration. Compact reactor optimization benefits substantially from modern computational methods that combine adequate physics fidelity with computational efficiency. Multi-group diffusion theory, properly implemented with sufficient energy resolution and inclusion of important physics effects such as temperature dependence and thermal up-scatter, provides accurate and computationally efficient optimization capability. The two-stage optimization algorithm reduces computational cost by 40 percent while maintaining accuracy, enabling parametric studies and uncertainty quantification that would prove prohibitively expensive with less efficient methods or higher-fidelity Monte Carlo approaches for every parameter evaluation.

Medical isotope production facilities require fundamentally multi-objective design thinking that departs from traditional single-objective reactor optimization. Maximizing production of any single isotope yields suboptimal performance when multiple isotopes with different spectral requirements must be produced simultaneously. The weighted portfolio approach balancing multiple isotope production rates according to clinical demand and economic value better serves actual facility missions than single-isotope optimization. This insight applies broadly to multi-product facilities and suggests that conventional optimization approaches may systematically miss superior design points by failing to properly account for multiple simultaneous objectives.

Beryllium retains its position as an excellent reflector material for compact high-flux applications despite well-known challenges including poisoning, swelling, and high cost. The unique combination of low absorption cross-section, high scattering cross-section, and solid form at room temperature provides performance characteristics unmatched by alternative reflector materials. While poisoning and swelling limit reflector lifetime and require eventual replacement, operational experience spanning decades demonstrates that these challenges can be successfully managed through

appropriate design provisions, operational procedures, and maintenance planning. The substantial production enhancements enabled by optimized beryllium reflectors provide strong economic justification for accepting these operational complexities.

Nuclear data uncertainties remain significant even among modern evaluated libraries incorporating decades of measurement programs and sophisticated evaluation methodologies. The 5 to 11 percent variations between contemporary libraries for beryllium-reflected systems indicate continued need for experimental validation programs, evaluation methodology improvements, and realistic uncertainty quantification in design calculations. Designers must recognize that calculation uncertainties from nuclear data often exceed uncertainties from computational methods or modeling approximations, and design margins should account for these irreducible uncertainties in current knowledge of nuclear interaction probabilities.

Practical Recommendations

For designers and operators of new medical isotope production reactors, several specific recommendations emerge from this comprehensive analysis. New facility designs should begin with an initial reflector thickness of approximately 12.5 centimeters corresponding to the balanced optimization configuration, providing excellent overall performance across multiple objectives. Incorporation of variable thickness top reflector capability enables long-term burnup compensation without fuel element modifications, following proven operational model from Miniature Neutron Source Reactor experience. Control systems should be designed to accommodate excess reactivity in the range of 500 to 700 pcm, providing adequate range for operational flexibility while avoiding excessive reactivity that complicates safety analysis and licensing. High-purity beryllium exceeding 98 percent purity should be specified to minimize parasitic absorption and maximize reflector performance, with the incremental cost easily justified by performance improvements. Reflector replacement planning should anticipate operational lifetime of 10 to 15 years at full power operation before dimensional swelling or poisoning effects necessitate replacement, with provisions for interim monitoring and assessment.

For existing reactor facilities considering reflector modifications or optimization, current configurations should be evaluated against the Pareto frontier identified in this work to determine proximity to optimal performance. Facilities whose current reflector thickness lies within 2 centimeters of the identified optimum may find that modification costs exceed benefits from marginal performance improvements, while facilities with substantially suboptimal configurations may justify major modifications. Beryllium poisoning monitoring programs should track reactivity evolution over time to validate predictions and inform replacement planning decisions. Comprehensive reflector replacement strategies should be developed addressing safety during removal of activated and potentially tritium-contaminated materials, minimization of facility downtime during replacement operations, and disposition of removed reflector material in accordance with radioactive waste regulations.

For reactor physics analysts performing design calculations for beryllium-reflected systems, several methodological recommendations ensure adequate accuracy. Energy group structure should employ minimum 10 groups with enhanced thermal resolution for medical isotope production applications, as traditional 4 to 7 group structures prove inadequate for accurate production rate calculations. Temperature-dependent cross-sections incorporating Doppler broadening at operating temperatures should be included rather than room-temperature evaluations, with temperature corrections of several percent proving significant for safety and production calculations. The JENDL-3.2 nuclear data library should be employed for beryllium-moderated and reflected systems based on demonstrated superior agreement with experimental data, though sensitivity studies with alternative libraries provide useful uncertainty bounds. Final critical designs should incorporate validation through higher-fidelity Monte Carlo calculations using detailed geometric models to confirm diffusion theory results and quantify approximation errors, particularly for novel geometries or unusual configurations where diffusion theory approximations may introduce larger uncertainties.

Limitations of Current Work

The present analysis contains several simplifications and approximations that should be recognized when applying results to practical design situations. The two-dimensional cylindrical geometry employed in calculations simplifies actual three-dimensional reactor configurations, particularly axial reflector effects and geometric details. Asymmetries in actual reactor designs including control rod penetrations, irradiation channels, and structural components introduce local perturbations not captured in idealized axisymmetric models. The homogenized core representation neglects fuel pin heterogeneity and its effects on local flux distributions and self-shielding. Individual fuel pins exhibit strong local flux variations not resolved in homogeneous core models, potentially affecting production calculations for targets located within fuel elements.

Static analysis without time-dependent phenomena provides adequate accuracy for initial design optimization but neglects important operational transients. Xenon and samarium fission product poisoning evolution following power changes significantly impacts short-term reactivity behavior and operational procedures. Beryllium poisoning accumulation occurs continuously during operation, creating slowly evolving reactivity trends requiring long-term compensation. These dynamic effects receive only parametric treatment in the present analysis rather than fully coupled time-dependent simulation. Thermal-hydraulic phenomena including coolant temperature distributions, natural circulation patterns, and heat transfer mechanisms operate independently from neutronics calculations in this work. The assumption of uniform

constant temperatures within each material region simplifies actual complex temperature distributions that influence cross-sections and material properties through thermal expansion.

Mechanical behavior of beryllium including thermal expansion, radiation-induced swelling, and stress distributions receives no treatment in the present analysis. Dimensional changes from swelling potentially affect geometric parameters and create mechanical loads on structural components. Residual stresses from fabrication and cyclic thermal loading may influence long-term mechanical integrity. These mechanical effects may ultimately limit reflector lifetime even before neutronic degradation becomes limiting. Recognition of these limitations guides appropriate application of results and identifies areas requiring additional analysis for final detailed design.

Recommended Future Work

Several natural extensions of the present work would substantially advance understanding and design capability for beryllium-reflected medical isotope production reactors. Short-term research priorities should address the most significant limitations of current analysis. Three-dimensional geometric modeling incorporating full axial reflector configuration, control rod channels, irradiation positions, and structural details would provide more realistic flux distributions and enable optimization of component placement. Heterogeneous core modeling with explicit fuel pin geometry would improve accuracy of local flux calculations and enable investigation of optimal fuel loading patterns. Coupled depletion calculations tracking fuel burnup, fission product accumulation, and beryllium poisoning evolution over operational cycles of 1 to 5 years would provide comprehensive understanding of time-dependent behavior. Monte Carlo validation calculations using codes such as MCNP or SERPENT with continuous-energy cross-sections and detailed geometric models would confirm diffusion theory results and quantify systematic approximations.

Medium-term research initiatives should address multi-physics coupling and material behavior effects currently neglected. Thermal-hydraulic coupling integrating neutronics with codes such as RELAP5 or TRACE would provide self-consistent temperature distributions accounting for power deposition patterns, coolant flow characteristics, and heat transfer mechanisms. Mechanical stress analysis incorporating radiation-induced swelling, thermal expansion, and structural loads would predict dimensional evolution and assess structural integrity throughout reflector lifetime. Detailed spatial modeling of beryllium poisoning including three-dimensional distributions of Helium-3 and Lithium-6 would improve predictions of local neutronic effects and inform reflector management strategies. Economic optimization incorporating full lifecycle costs including initial capital, operating expenses, maintenance costs, and eventual disposal would enable more complete assessment of design alternatives.

Long-term research directions should pursue advanced analysis capabilities and experimental validation. Comprehensive multi-physics coupling integrating neutronics, thermal-hydraulics, and mechanical behavior in unified simulation framework would provide holistic system performance prediction. Stochastic optimization with explicit uncertainty quantification would propagate nuclear data, manufacturing tolerance, and modeling uncertainties through design calculations to provide confidence intervals on performance predictions. Machine learning surrogate models trained on high-fidelity simulation results could enable rapid parameter exploration across high-dimensional design spaces currently inaccessible due to computational expense. Experimental validation programs including targeted irradiation tests of beryllium specimens and benchmark measurements in operating facilities would provide essential data for model validation and uncertainty reduction, strengthening confidence in computational predictions for novel designs.

Closing Perspective

As global demand for medical radioisotopes continues growing while the fleet of aging research reactors gradually diminishes, optimized compact reactor designs become increasingly important for ensuring reliable supply of these life-saving materials. This comprehensive framework for beryllium reflector optimization addresses critical design questions through rigorous physics-based analysis and multi-objective optimization methodology. The quantified performance improvements, validated against operational experience, provide practical guidance for both new facility designs and existing facility upgrades.

The optimal configuration identified through this analysis, featuring 12 to 15 centimeter beryllium reflector thickness, achieves excellent balance between production maximization, safety maintenance, and cost control. This design point enables facilities to maximize their contribution to global medical isotope supply while maintaining safe, reliable, and economical operation. By providing designers with comprehensive tools for making informed decisions balancing competing objectives, this work ultimately supports the reliable production of radioisotopes serving millions of patients worldwide who depend on nuclear medicine for disease diagnosis and treatment.

The broader methodological contributions advance the state of computational reactor design by demonstrating the value of adequate physics fidelity, comprehensive nuclear data comparison, and systematic multi-objective optimization. These approaches prove applicable beyond medical isotope production to diverse reactor applications requiring careful balance of competing performance objectives. As nuclear technology continues evolving to address societal needs including medical applications, research applications, and potential future energy systems, sophisticated design optimization frameworks incorporating multiple physics, multiple objectives, and comprehensive uncertainty treatment will prove increasingly essential for realizing optimal performance from advanced nuclear systems.

References

1. OECD-NEA, "The Supply of Medical Radioisotopes: 2019 Medical Isotope Demand and Capacity Projection for the 2019-2024 Period," NEA No. 7499, 2019.
2. International Atomic Energy Agency, "Non-HEU Production Technologies for Molybdenum-99 and Technetium-99m," IAEA Nuclear Energy Series No. NF-T-5.4, Vienna, 2013.
3. Sesonske, A., & Glasstone, S. (1994). Nuclear reactor engineering. Chapman & Hall.
4. Lamarsh, J.R., "Introduction to Nuclear Engineering," 2nd Edition, Addison-Wesley, 1983.
5. Tomberlin, T. A. (2004). Beryllium–A Unique Material in Nuclear Applications,‖ Idaho National Engineering and Environmental Laboratory. Idaho Falls, ID.
6. Hausner, H. H. (1963). Beryllium as a moderator and reflector for nuclear reactors.
7. Knoll, G.F., "Radiation Detection and Measurement," 2nd Edition, John Wiley & Sons, 1989.
8. Muhammad, S. T., Chaudri, K. S., & Ahmad, A. (2008). Beryllium as reflector of MNSR. Annals of Nuclear Energy, 35(9), 1708-1712.
9. Omar, H., Ghazi, N., Haddad, K., & Ezzuddin, H. (2012). Study the effect of beryllium reflector poisoning on the Syrian MNSR. Applied Radiation and Isotopes, 70(6), 988-993.
10. Wroblewska, M. (2017). Beryllium Poisoning Model for Research Reactors. RRFM, May, 14-18.
11. Andrzejewski, K. J., & Kulikowska, T. A. (2004). Isotopic transmutations in irradiated beryllium and their implications on Maria reactor operation. Nuclear technology, 146(1), 72-82.
12. Van Renterghem, W., Leenaers, A., & Van denBerghe, S. (2008). TEM investigation of long-term annealed highly irradiated beryllium. Journal of nuclear materials, 374(1-2), 54-60.
13. Lemmel, H.D., McLaughlin, P.K., and Pronyaev, V.G., "Summary of Contents, ENDF/B-VI, Release 8," IAEA Nuclear Data Section, 2001.
14. Nakagawa, T., Shibata, K., Chiba, S., Fukahori, T., Nakajima, Y., Kikuchi, Y., ... & Asami, T. (1995). Japanese evaluated nuclear data library version 3 revision-2: JENDL-3.2. Journal of Nuclear Science and Technology, 32(12), 1259-1271.
15. JEFF-3.1 Nuclear Data Library, NEA Data Bank, www.nea.fr/html/dbdata/JEFF/, 2005.
16. Wikipedia Contributors, "Beryllium," Wikipedia, The Free Encyclopedia.
17. Behrens, R.G. et al., Beryllium: Environmental Analysis and Technology Assessment, 2003.
18. Romano, P. K., & Forget, B. (2013). The OpenMC monte carlo particle transport code. Annals of Nuclear Energy, 51, 274-281.
19. OpenMC Development Team, "OpenMC: An Open-Source Monte Carlo Particle Transport Code," MIT, 2023.
20. Cacuci, D.G. (Ed.), Handbook of Nuclear Engineering, Springer, 2010. (Beryllium moderator properties.)
21. Abdollahzadeh, M. Y., & Boroushaki, M. (2009). Using nodal expansion method in calculation of reactor core with square fuel assemblies.
22. Jamalabadi, M.Y.A.Constructal theory of critical mass, Int. J. Nuclear Energy Scienceand Technology, accepted for publication.
23. Jamalabadi, M. Y. A. (2025). Thermohydraulic Safety Analysis of a Research Reactor by Transport in Porous Media Technique. Evolutions Mech Eng, 6(2), 1-11.
24. Jamalabadi, M. Y. A. (2026). Numerical investigation of induction hardening of stationary cylindrical steel pins with convective quenching. Mechanical Engineering Advances, 4(1).
25. Jamalabadi, M.Y.A, Using Nodal Expansion Method in power Calculation of pressurized water reactor (PWR) Core with Square Fuel Assemblies, MSC thesis, Sharif University of technology 2008
26. M.Y.A. Jamalabadi ,Design of Quadrupole Mass Spectrometer for fundamental Particle, Fundamental Physics Seminar, (2026)
27. Abdollahzadeh Jamalabadi, S. A. (2026). Molecular Key to the Filter: Podocin Phosphorylation Unveiled in a Case of Early-Stage Steroid-Resistant Nephrotic Syndrome. Ann Clin Med Case RepŪ, 15(1), 1-11.
28. M.Y.A. Jamalabadi ,Design and Thermal Analysis of a Semi-Passive Thermal Control System for a Student Satellite , (2026) 1–181
29. Abdollahzadeh Jamalabadi, M. Y. (2026). Perturbative Manipulation of Neutrino Flavor: A Predictive A4 Model with a Vanishing Determinant. Available at SSRN 6169528.
30. Jamalabadi, M. Y. A. (2026). Numerical investigation of induction hardening of stationary cylindrical steel pins with convective quenching. Mechanical Engineering Advances, 4(1).